

DTIC FILE COPY

AD-A196 375

SECURITY CLASSIFICATION OF THIS PAGE (When Data Entered)

REPORT DOCUMENTATION PAGE		READ INSTRUCTIONS BEFORE COMPLETING FORM
1. REPORT NUMBER AFIT/CI/NR 88-2	2. GOVT ACCESSION NO.	3. RECIPIENT'S CATALOG NUMBER
4. TITLE (and Subtitle) TROPICAL 200 mb DIVERGENT CIRCULATIONS AND THEIR RELATION TO OUTGOING LONGWAVE RADIATION		5. TYPE OF REPORT & PERIOD COVERED MS THESIS
AUTHOR(s) FRANK SORNATALE		6. PERFORMING ORG. REPORT NUMBER
PERFORMING ORGANIZATION NAME AND ADDRESS AFIT STUDENT AT: UNIVERSITY OF MARYLAND		10. PROGRAM ELEMENT, PROJECT, TASK AREA & WORK UNIT NUMBERS
CONTROLLING OFFICE NAME AND ADDRESS		12. REPORT DATE 1988
14. MONITORING AGENCY NAME & ADDRESS (if different from Controlling Office) AFIT/NR Wright-Patterson AFB OH 45433-6583		13. NUMBER OF PAGES 73
		15. SECURITY CLAS. (of this report) UNCLASSIFIED
		15a. DECLASSIFICATION/DOWNGRADING SCHEDULE
16. DISTRIBUTION STATEMENT (of this Report) DISTRIBUTED UNLIMITED: APPROVED FOR PUBLIC RELEASE		
17. DISTRIBUTION STATEMENT (of the abstract entered in Block 20, if different from Report) SAME AS REPORT		
18. SUPPLEMENTARY NOTES Approved for Public Release: IAW AFR 190-1 LYNN E. WOLAVER <i>Lynn Wolaver 12 July 88</i> Dean for Research and Professional Development Air Force Institute of Technology Wright-Patterson AFB OH 45433-6583		
19. KEY WORDS (Continue on reverse side if necessary and identify by block number)		
20. ABSTRACT (Continue on reverse side if necessary and identify by block number) ATTACHED		

88 8 3

ABSTRACT

Title of Thesis: Tropical 200 mb Divergent Circulations and Their
Relation to Outgoing Longwave Radiation

Frank Sornatale, Master of Science, 1988

Thesis directed by: Anandu D. Vernekar, Professor,
Department of Meteorology

We present annual and interannual variability of the 200 mb level mean meridional circulations (Hadley and Ferrel cells) and 200 mb tropical east-west circulations (Walker circulations), as inferred from the velocity potential field. Also, we present a relationship between divergence at 200 mb and outgoing longwave radiation (OLR).

A major feature of the 200 mb tropical divergent velocity field is the dominance of the western Pacific monsoon region as the source for meridional and zonal overturning motions. Smaller, but significant similar source regions are found over South and Central America as well as central Africa. One significant variation is their intra-seasonal transitions to the summer hemisphere. The northern hemisphere circulations undergo more variations than those of the southern hemisphere.

Intra-annual variations of the equatorial Hadley cell are dominated by the variations of Asian Monsoon circulations. The seasonal fluctuations in

the divergent velocity field in the western Pacific contribute to a strong annual cycle in the inter-annual pattern in the tropics.

The results on east-west over-turning motions show that there are three cells associated with the three ascending branches over the Asian monsoon, South and Central America, and Central Africa. The most dominant cell is the Walker cell with its ascending branch over the western Pacific (Asian monsoon) and descending branch in the eastern equatorial Pacific. The intensity and location varies within the year. The inter-annual variability appears to be associated with the El Nino event.

The relationship between divergence and the equivalent blackbody temperature index, derived from OLR data, is significant in the tropical convective region. The relationship is weak in the subsidence region away from the tropical belt, 20° north or south.



Accession For	
NTIS GBA&I	<input checked="" type="checkbox"/>
DTIC TAB	<input type="checkbox"/>
Unrestricted	<input type="checkbox"/>
Justification	
By _____	
Distribution/ _____	
Availability Codes	
Dist	Available/On Special
R-1	

TROPICAL 200 MB DIVERGENT CIRCULATIONS
AND THEIR RELATION TO OUTGOING
LONGWAVE RADIATION

by

Frank Sornatale

Thesis submitted to the Faculty of the Graduate School
of the University of Maryland in partial fulfillment
of the requirements for the degree of
Master of Science
1988

Advisory Committee:

Dr. Anandu D. Vernekar
Dr. Robert E. Ellingson
Dr. George Huffman
Dr. Philip Arkin

To my children:

Stephanie Anne, Christina Anne, Frank Paul

ACKNOWLEDGEMENTS

I would like to thank my three children, Stephanie, Christina, and Frank Paul, for being the best children in the world. They gave me time to study which got me through the days, and a whole lot of love which got me through the nights.

I would also like to thank Dr. Anandu D. Vernekar, my research advisor, for his support in seeing that this thesis was completed. It is an extreme understatement to say I would not have received this degree if not for his assistance. I also want to single out the help of Dr. Philip Arkin, Chief, Climate Analysis Center, National Weather Service (NWS), who helped select this topic and provided all of the data used in the research. In addition, Dr. George Huffman and Dr. Robert Ellingson both provided very useful support and ideas relating to the analysis in this thesis.

Finally I would like to acknowledge the support of the United States Air Force and Air Weather Service for giving me the opportunity to attend graduate school. A special thanks to Brigadier General George Chapman, for supporting my request to attend school at an age beyond those of my peers.

Table of Contents

List of Figures	v
1. Introduction	1
2. Data	6
Velocity Potentials	6
Outgoing Longwave Radiation	10
Equivalent Black Body Temperature	12
3. Mean Seasonal Velocity Potential and OLR	14
4. Mean Meridional Circulation	30
5. Mean Zonal Circulations	38
6. 200 mb Divergence and EBBI Correlations	49
7. Summary	60
Appendix: Computational Techniques	69
References	67

List of Figures

1. Mean Velocity Potential & Irrotational Velocity Vectors	22
2. Mean EBBI & Irrotational Velocity Vectors	23
3. Mean Velocity Potential & Irrotational Velocity Vectors	24
4. Mean EBBI & Irrotational Velocity Vectors	25
5. Mean Velocity Potential & Irrotational Velocity Vectors	26
6. Mean EBBI & Irrotational Velocity Vectors	27
7. Mean Velocity Potential & Irrotational Velocity Vectors	28
8. Mean EBBI & Irrotational Velocity Vectors	29
9. Zonal Mean Merridional Velocity, 1979 - 1986	35
10. Intra-annual Mean Divergence and EBBI, 1979 - 1986	36
11. Inter-annual Mean Divergence and EBBI, 1979 - 1986	37
12. Mean Zonal Wind, DJF/JJA	43
13. Intra-annual Mean Zonal Velocity and EBBI	44
14. Inter-annual Mean Zonal Velocity and EBBI	45
15. Mean Zonal Irrotational Wind - January/July	46
16. Mean EBBI and Irrotational Wind Vectors, January	47
17. Mean EBBI and Irrotational Wind Vectors, July	48
18. Correaltions, EBBI and Divergence, Eq. - 5° N	53
19. Correaltions, EBBI and Divergence, 30° N - 25° N	54
20. Correaltions, EBBI and Divergence, 30° N - 30° S	55
21. Temporal Correlations, January: 120° W - 60° E	56

22. Temporal Correlations, January: 60° E - 120° W	57
23. Temporal Correlations, July: 120° W - 60° E	58
24. Temporal Correlations, July: 60° E - 120° W	59

Tropical 200 mb Divergent Circulations and Their Relation to Outgoing Longwave Radiation

1. Introduction

Large-scale tropical irrotational motions develop in response to differential heating in the atmosphere. The rotational motions are generated by the earth's rotational effects through the divergence term ($f + \zeta$) $\nabla \cdot \vec{V}$ in the vorticity equation where f is the Coriolis parameter and ζ is the relative vorticity. Because f is proportional to the sine of latitude, the effects of this term increases from the equator to the poles. While large scale motions in most of the atmosphere are dominated by rotational components, the irrotational motions are important in the tropics where the Coriolis parameter is small.

The tropics, which cover half the area of the globe, provides a large amount of the energy needed to drive the global circulations. The energy, in the form of sensible and latent heat, is transported towards the equator by the trade winds in the lower levels. This energy is then lifted and condensed, thereby providing sensible heat and potential energy which is transported poleward by the circulations of the upper troposphere. Deep cumulus convection is considered to be the major mechanism in the vertical transport of low level energy to the upper troposphere.

The theories of axially symmetric (zonally averaged) components of the general circulation of the atmosphere explain the maintenance of momentum, heat and water vapor in the atmosphere. Lorenz (1967) shows the contributions of mean meridional (Hadley) circulations in explaining these

maintenances. The mean meridional circulations, by definition, exist solely in divergent flow.

Bjerknes (1969) and Krishnamurti (1971a,1971b,1973) studied the axially asymmetric components of tropical circulations. These asymmetries are the result of variations in thermal and orographic forcing along the zonal plane. One component of these circulations is the zonal over-turning motion in the equatorial Pacific Ocean. Bjerknes referred to the pressure and temperature oscillations supporting this circulation as the Southern Oscillation.

The Southern Oscillation (SO) is a dipole structure in the pressure pattern with centers located in the tropical eastern and western Pacific Ocean. The steepness in the pressure gradients between the centers is a measure of intensity of these over-turning circulations. Bjerknes (1969) and Arkin (1982) have shown this relationship using the 200 mb tropical wind field and the Southern Oscillation Index (SOI) which is a measure of surface pressure gradients. They also show an association between the SOI and the equatorial Pacific sea surface temperature (SST).

Bjerknes (1969) renewed interest in this zonal circulation when he described the characteristics of this thermally driven cell he called the Walker circulation. Krishnamurti (1973) went on to characterize this local Pacific circulation as one branch of a more extensive east-west circulation he found extending across the entire circumference of the equatorial belt. The Walker circulation is very important to both the tropical and extra-tropical circulations. It is maintained by rising air in the western Pacific 'source'

region of warm sea surface temperatures and descending air over the eastern Pacific 'sink' where the sea surface temperature is relatively cold. Warm and moist air is drawn into the western Pacific low level convergence center, rises in its ascending column, and empties the mass of air into an upper-tropospheric horizontal divergence center. The air from this divergence center becomes part of the 200 mb Hadley and Walker circulations. The Walker branch circulates back into the 200 mb convergence center supporting the eastern Pacific 'sink'. The low-level divergence out of the base of this 'sink' increases the easterly winds which in-turn cools the SST by upwelling affects. This cooling creates a stronger SST gradient between the source and sink regions which is associated with the intensification of the Walker circulation.

In mid-latitudes, rotational components are normally an order of magnitude larger than irrotational components. In the tropics, however, the irrotational component is approximately of the same order as rotational components. The tropical upper-tropospheric irrotational circulation drives both the global meridional and the tropical zonal circulations. Several studies of this circulation include those by Paegle and Paegle (1978), Cressman (1981), and Chang and Lau (1982). They have studied the variability of tropical circulations with particular attention to sub-tropical jet stream enhancement in areas of upper-tropospheric convergence. In a recent study, Lau and Boyle (1987) show the relationship between the variability of the horizontal divergence field and the strength of the sub-tropical jet stream.

Studies of horizontal divergence have been limited by the availability

of accurate observations. Conventional ground-based observations are limited in space and time because of the scarcity of observation sites over oceans and in the third world countries which are heavily populated the tropical belt. The usefulness and accuracy of satellite-derived winds, as with most indirect measurements, has some serious problems which restrict its use. Hubert and Whitney (1971) identified several possible error sources, including: errors due to uncertainties of cloud heights, errors due to non-advectional cloud motions, errors of measurement, and errors in tracking cloud targets. These deficiencies have led to other sources for wind field data.

A source currently under investigation is the use of data from NOAA polar orbiting satellites which provide a full spatial distribution of the net outgoing longwave radiation (OLR) from twice daily measurements. The tops of deep convective clouds, because of their cold cloud-top temperatures and high emissivity, emit lower radiation than the earth's warm surface under clear skies. Therefore, in the tropics, OLR fields can be used to infer low-level convection supporting deep cumulus cloud structures. Rupert and Gray (1976) showed a large positive correlation between the intensity of convection associated with tropical upper-tropospheric cloud clusters and horizontal divergence. From these observations one may use OLR as a proxy for low-level convergence or upper-tropospheric divergence.

Since 1974 several studies have tried to estimate kinematic fields from OLR data. Julian (1984) and Kasahara et. al. (1987b) have utilized OLR to improve the accuracy of the initial field used in numerical weather prediction by deriving irrotational components of wind from OLR data. These

studies were attempting to establish a relationship between OLR and tropical divergent winds on a daily basis. Their results show only limited success.

The purpose of this study is to understand the variability of the tropical 200 mb divergent circulation. At the same time we seek a relationship between the monthly mean OLR and 200 mb horizontal divergent winds. Towards this end, we analyze the intra- and inter-annual variabilities in the 200 mb divergent wind field and relate them to variabilities in the OLR field. Chapter 2 gives a brief description of both data sets and their origins. Variations in the seasonally averaged data, the zonal and time-mean zonal average of the irrotational winds' meridional component, and the meridional and time-mean meridional average of the irrotational winds' zonal component are shown in Chapters 3, 4, and 5 respectively.

In Chapters 3 to 5 we use independent OLR data in the form of OLR and Equivalent Black Body (EBB) temperature indexes, as a proxy for convection to assess our results from the velocity potential data. Finally, in Chapter 6 we do a correlation analysis between the 200 mb divergence and EBB indexed data to quantify the relationship between the monthly mean fields.

2. Data

a. Velocity Potentials

The velocity potential data used in this study is a 2.5° globally grid-ded field provided by the National Meteorological Center (NMC), Climate Analysis Center (CAC) in the form of ninety-six monthly means covering the period from January 1979 to December 1986. Averaging was done twice daily for the 00Z and 12Z runs of the Global Data Assimilation System (GDAS) used at the NMC.

Prior to 1978 the GDAS used a Hough analysis technique which contained no divergent motions. On 22 September 1978 the Hough analysis was replaced by an Optimal Interpolation (OI) process w¹ich does include divergence. Kistler and Parish (1978) describe the three major components of the GDAS in detail. They consist of analysis, initialization and prediction. Prediction is only indirectly relevant to this study and will not be discussed.

Under this OI scheme, the objective of data analysis is to determine the values of meteorological variables at regularly spaced grid points from sparse sets of randomly spaced observations. Compounding the problem, each observation system has its own level of accuracy in reporting the data. Interpolation methods based on statistical techniques are used to do this interpolation in the sigma coordinate frame of the prediction model. Since meteorological observations can not provide a reasonably populated initial field of data, the 6-hr forecast from the previous numerical model's run is used as the first guess field by the GDAS.

Spatial interpolation are used to match randomly located observed data to the same globally gridded resolution as the first guess field. This guess field is then subtracted from the observed field to form a difference field used in further processing. The final raw analysis is produced by linearly combining the difference and the first guess field. The combination is weighted by quality assessment for the various observations. The result field is a new (corrected) analysis field.

Numerical models have a hard time utilizing data which are not consistent with the governing equations of the model. Any inconsistencies with the particular model's mass motion balance requirements produces inertial gravity waves which the model might treat as a perturbation in the flow. As a perturbation, numerical models may allow the very small gravity wave to grow to orders of magnitude greater than its actual strength in the real atmosphere. Because of this potential to distort this type of data, it is important to filter out these inconsistencies before the model integration begins. This filtering occurs in the initialization phase.

The initialization process consists of interpolation techniques and mass-motion balance requirements which have undergone several changes between January 1979 and December 1986. On 27 May 1980 the GDAS converted from a 9-layer global gridpoint domain to a 12-layer, 24-wave, global spectral model. This change reduced the problems associated with inconsistencies in the data described above and according to Kistler and Parish (1982) it improved wind forecasts. On 14 August 1982 an isobaric multi-variate OI (MOI) scheme was implemented which expanded the model

from 24 to 30 waves. Dey and Morone (1985) give the full details of the MOI system which they found improved the upper-tropospheric wind forecast.

Adiabatic initialization using geostrophic assumptions were used until September 1984. This made the difference field consistent with the GDAS first guess field which is also based on geostrophic assumptions. These assumptions weaken the magnitude of divergence, causing a dampening of the Hadley and Walker circulations produced by the analysis. In addition, diabatic heating accumulates during the first 24 hours of the model's integration. The lack of diabatic heat suppresses vertical motions in the barotropic tropics which further inhibits the formation of thermally direct cells.

In September 1984 the adiabatic initialization process was replaced by a diabatic non-linear normal mode initialization (NNMI) process. Mohanty et. al. (1986) reported this improves the vertical consistency of the model and improves the accuracy in the placement of tropical convective systems.

In May of 1986 major changes to the GDAS were made to both the analysis procedures and to the global forecast model. The analysis changes included expanding corrections to a 40-wave rhomboidal truncation, increasing the number of observations affecting a correction from 20 to 33, and including TIROS sounding data over land (above 100 mb). At the same time the global spectral prediction model was replaced by an upgraded spectral model used to make medium range forecasts. This version expands the horizontal resolution from 30 to 40 waves while the vertical resolution is

increased from 12 to 18 sigma layers. New physical parameterizations replaced less sophisticated procedures of the older global spectral model. The reader is directed to the report by Dey et. al. (1987) for the specifics of all the changes implemented at this time.

The procedure for separating wind vectors into rotational and irrotational components is described in detail by Dey and Brown (1976). The 'Helmholtz theorem' is used to break a velocity vector into its components:

$$\vec{V} = \vec{k} \times \nabla \Psi + \nabla \chi \quad (1)$$

where Ψ is the stream function (rotational), χ is the velocity potential (irrotational), and ∇ is the horizontal gradient operator. Dey and Brown (1976) applied this theorem with finite differencing methods to compute the rotational and irrotational wind components:

$$\zeta = \nabla^2 \Psi \quad (2)$$

$$D = \nabla^2 \chi \quad (3)$$

where D is the divergence and ζ is the relative vorticity. In this study we have chosen the convention

$$-D = \nabla^2 \chi \quad (4)$$

This convention reverses the signs of the original χ data from NMC, which followed the conventions of Dey and Brown. In our study positive values represent divergence and negatives represent convergence. The irrotational wind component was computed from the velocity potential field using the

following finite differences:

$$u_x = \frac{1}{a \cos \phi} \frac{\partial \chi}{\partial \lambda} \approx \frac{1}{a \cos \phi} \left(\frac{\chi_{i+1,j} - \chi_{i-1,j}}{2 \Delta \lambda} \right) \quad (5)$$

$$v_x = \frac{1}{a} \frac{\partial \chi}{\partial \phi} \approx \frac{1}{a} \left(\frac{\chi_{i,j+1} - \chi_{i,j-1}}{2 \Delta \phi} \right) \quad (6)$$

We compared our calculations with those of Dey and Brown and found they were identical.

b. Outgoing Longwave Radiation (OLR)

The OLR data used in this study are total flux estimates obtained from the NOAA polar-orbiting satellite series which are low orbiting, sun-synchronous satellites, operating since 1974. The data were digitized on a 2.5° global grid and consist of mean monthly values calculated from twice-daily observations collected from January 1979 to December 1986.

The Advanced Very High Resolution Radiometer (AVHRR) aboard the NOAA Polar Orbiters measures the earth's terrestrial radiation budget in the 10 - 12.5 μm window. These narrow band measurements are used to estimate the total outgoing flux over the full spectrum by applying empirical relationships developed by Abel and Gruber (1979). The collection and interpolation process has several areas of bias which we will summarize here.

One bias exhibited by the satellites is discussed by Gruber and Kruger (1984) and concerns changes in the equatorial crossing times of different satellites. During this period crossing times varied from the early 0230-1430 LST crossings of NOAA7 to the late 0730-1930 LST crossings of NOAA-6.

These variations would be especially noticeable over the sub-tropical desert regions where a crossing during the peak heating of afternoon (1430 LST) would cause a positive bias in the flux measurement. Because this study uses monthly means from twice daily averaged measurements, we assume the affects of these variations should not be significant.

Another bias is in the over-estimate of flux values. One reason is discussed by Ramanathan and Briegleb (1980) based on the effects of cirrus clouds. Cirrus clouds are semi-transparent in the infra-red region which lowers their emissivity which causes an over-estimate in the flux measurements. Related over-estimates investigated by Ellingson and Ferraro (1983) and Ohring et. al. (1984) amounted to a 10 W m^{-2} from middle and high partial cloudiness. In this study we use monthly mean values which we assume reduces the occurrence of false readings from these over-estimates.

In this study we use OLR indexes to infer the location of low-level convergence and their associated upper-tropospheric divergence centers. The procedures we use provide an index from which we can infer the intensity and locations of convection and the kinematic motions associated with it. Similar inferences between maxima in the OLR data and upper-tropospheric convergence centers are not as reasonable (see Kasahara et. al., 1987b). Clear skies implied by the maxima can be caused by several mechanisms including: dry convection found over deserts, upper-tropospheric subsidence, or neutral activity (neither convection or subsidence).

Furthermore, the link between convection and OLR is only valid in the tropics where vertical motions are proportional to the diabatic heating. Fol-

lowing the scaling arguments of Holton (1979), both the local temperature variation and the temperature advection term in the tropics are negligible, so we can reduce the thermodynamic equation:

$$\left(\frac{\partial}{\partial t} + \nabla \cdot \nabla \right) T - \omega S_p = \frac{\dot{q}}{c_p} \quad (7)$$

to

$$\omega = \frac{\dot{q}}{S_p c_p} \quad (8)$$

where S_p is the static stability term, \dot{q} the rate of diabatic heating, and ω the vertical-p velocity. In tropical precipitating systems the vertical velocity is $\approx 3 \text{ cm s}^{-1}$, which is an order of magnitude larger than outside of the precipitation regions. In the extra-tropics the temperature advection can not be neglected hence the relationship we have established here between OLR and kinematic motion is not valid. Therefore, our discussions are generally confined to the tropical belt between 30°N and 30°S .

We use an indexing method to highlight convection inferred by the lowest flux measurements and the clear skies by the highest fluxes. By subtracting OLR flux from the median tropical flux (240 W/m^2) we can highlight maxima and minima in the OLR field.

$$\text{OLR Index (OLRI)} = 240 \text{ W/m}^2 - \text{OLR Flux} \quad (9)$$

In this index, sign conventions have convection inferred in the maxima and clear skies in the minima. This conforms to conventions for 200 mb divergence derived from velocity potential data.

c. Equivalent Black Body (EBB) Temperature (T_e)

Several studies, including those of Julian (1984) and Kasahara et. al. (1987b), use Equivalent Blackbody (EBB) temperature (T_e) to study the relationship between divergence and OLR. The EBB temperature is computed using the 'Stephan-Boltzman law':

$$T_e = \left(\frac{\text{Flux}}{\sigma} \right)^{\frac{1}{4}} \quad (10)$$

where σ is the Stephan-Boltzman constant ($5.6693 \times 10^{-8} \text{ W m}^{-2} \text{ K}^{-4}$).

We compute the EBBI by the following method:

$$\text{EBB temperature index (EBBI)} = 258^\circ\text{K} - T_e \quad (11)$$

The 258°K threshold was found by Kasahara (1987a) to be the T_e separating rising and sinking motions. This method conforms the EBBI sign convention to those described for OLRI above.

3. Mean Seasonal Velocity Potential and OLR

In this chapter we present the mean seasonal variations of velocity potentials and Outgoing Longwave Radiation (OLR) for the 8 years from January 1979 to December 1986. As described in Chapter 2, the velocity potential field was affected by four changes in analysis procedures. In proceeding with our computations we assumed these changes only affect the amplitudes of the data but not the phases.

In this chapter maxima in the velocity potential, OLRI, and EBBI fields, denote low level convergence and upper-tropospheric horizontal divergence. Irrotational velocity vectors computed from the velocity potential field (see Appendix) have been superposed on figures in this section. The seasons we refer to are based on the northern hemisphere as follows: winter from December to February (DJF), spring from March to May (MAM), summer from June to August (JJA), and fall from September to November (SON).

Figure 1 shows the mean DJF distribution for the velocity potential and OLRI fields. The major feature in velocity potential is the High-Low dipole found in the tropical belt which dominates the global pattern. The irrotational vectors indicate the Borneo-Indonesia maritime continent in the southwest Pacific, which we will refer to as the Pacific Maritime Continent (PMC), is the central location for the major north-south (Hadley) and east-west overturning motions. The activity in the velocity potential field compares favorably with the OLRI field which shows the major convection region in the vicinity of the PMC. Smaller convection areas are also found

over south-central Africa and central South America.

Figure 2 magnifies the tropical features of the EBBI field during DJF with the irrotational vectors superposed. The dominant center of inferred convection from the EBBI field is over the PMC with a narrow zone extending to the east along the northwest coast of Australia and then to the southeast. The strongest velocity vectors originate from the PMC and their magnitude indicates the strength of the north-south overturning motions. The strongest 200 mb divergent winds flow towards the northwest where Figure 1 shows convergence into the 200 mb sink over Tibet. This convergence should be accompanied by a strong local minima in the OLRI field. Instead, a local maxima appears because of the high altitude. The surface temperatures in the Himalayas under clear skies are very cold which cause low OLR flux values. This is one example where topographic effects negate our general assumption inferring convection from minima in OLR flux.

Another major feature is the east-west circulations extending from the PMC. One branch flows towards the upper-tropospheric sink in the south Pacific convergence Zone (SPCZ) and another to the sink off the east coast of Africa. A second east-west flow extends from the South American convective center to the west coast of Africa. These east-west overturning motions on the zonal plane will be looked at more closely in section 5.

Several interesting features are observed in Figure 2 around Central and South America. The EBBI field infers convection over central South America which is also reflected in the irrotational velocity vectors. The irrotational velocity vectors also show strong convergence zones extending from

the Caribbean Sea to the western Atlantic Ocean, and off the coast of Venezuela. The EBBI field infers convection over south-central Africa and clear skies over north-central Africa. The irrotational velocity vectors show a convergence sink at 200 mb off the southeast African coast.

We compared our results with a similar study by Lau and Boyle (1987) which showed the mean velocity potential and irrotational wind vectors for the 9 DJFs from 1974/75 to 1982/83. The general patterns in the two studies agreed, especially the divergence pattern associated with the PMC. There are some differences however, mainly in the intensity of the irrotational wind vectors over South America, the Caribbean, and the western Pacific. There was also some disagreement on the spatial placement of several minor centers of minima and maxima values. We attribute these disagreements to differences in the data sets between the two studies.

Figures 3 and 4 compare the data fields for MAM. The maximum velocity potential in the PMC decrease from 9.2 m/s^2 in DJF to 7.25 m/s^2 in MAM. Accompanying the decrease are weaker irrotational winds which decrease from 4.4 m/s to 2.37 m/s . The irrotational winds are more symmetric about the equator than they were during DJF and the dominant flow pattern is now directed to the south and southeast out of the PMC. The core of the 200 mb divergence shifted to the north and a minima in velocity potential appears off the west coast of South America.

The OLRI pattern shows a northward drift of the PMC convection while a decrease in velocity potential gradients is apparent. The convection implied by OLRI maxima over South America and Africa covers less area

than in DJF.

The details of Figure 4 show a realignment and intensity drop-off in convection implied by the decrease in the PMC EBBI from 18°K in DJF to 15°K in MAM. The lower index value shows the top of the convection is at a lower level in the atmosphere and radiates at a warmer temperature than those with higher index values. From the weaker convection we infer that supporting kinematic motions are also weaker, specifically the horizontal divergence at the outflow of the convection. The 200 mb divergence, reflected by the irrotational wind field, has moved to the north and the magnitude of the flow has decreased since DJF. The local centers over South America and Africa have also undergone some realignment since DJF having moved approximately 5° to the north. There is stronger convergence off the west coast of South America than in DJF but the convergence center off the northwestern coast has decreased considerably. The EBBI field implies strong convection in central Africa and convergence in northeast Africa. These patterns are not clearly visible in the irrotational wind field.

The JJA patterns are shown in figures 5 and 6. The 200 mb divergence center over the PMC continues to move northward to approximately 10°N. The OLRI inferred convection supporting this circulation appears to be bordering the equator but extending away from the PMC toward the Southeast Asian peninsula. The maximum horizontal divergent velocity vector is 4.98 m/s which is the stronger than during any other season.

During the transition from MAM to JJA the effects of the summer monsoon become evident. Over the latter part of the MAM season, when

south Asia is warming and the Southern Hemisphere is cooling, the pressure gradients force air northwards forming a Low pressure system over southeast Asia. This is accompanied by increased rainfall over Burma and rising temperatures over India. The cycle breaks in late May to early June, with intense storm activity moving to the northeast from Burma. This monsoon cycle is visible in our figures even though the data is a three-month average.

Figure 5 shows that the summer monsoon has moved northwards across the equator and broadened considerably since MAM. The convection now extends from the PMC northeastward encompassing the Indian Ocean, Southeast Asia, and the Indian subcontinent. The narrow zone of convection in the central Pacific is seen in the EBBI pattern paralleling the equator at 10° N latitude, which is the preferred location of the inter-tropical convergence zone (ITCZ) during JJA. The EBBI pattern at 30° N 150° W indicates an area of clear skies which is persistent through all seasons but has its most extreme values in this JJA pattern.

Two east-west overturning circulations come from the summer monsoon convection. One branch is in the NH moving toward the west coast of Mexico, and a second is moving in the SH toward the west coast of South America. Very strong zonal irrotational winds flow from the summer monsoon towards the west coast of Africa.

The northwestward shift in convection is very noticeable in the EBBI patterns over South America. The inferred convection has moved from central South America in DJF to the Central American isthmus in JJA. In

addition, it has developed an elongated shape from Venezuela to the coastal waters of Baja Mexico in alignment with this land mass. The divergent velocity vectors show support for this inferred convection and the clear sky region near the SPCZ.

In MAM the elongated maxima in the EBBI pattern over Africa has split into two cells. Divergent velocity vectors flow from this convection to the upper-tropospheric convergent zone off the southwestern coast. There is also support in the irrotational winds for the central African convection and the 200 mb convergence zone in northeast Africa and Pakistan.

The final figures (7 and 8) show the mean SON season. There is a gradual shift in the activity back to the south and a weakening in magnitudes of both fields from the JJA maxima. Figure 8 clearly shows a long streak of inferred convection across the Pacific in the position of the Inter-Tropical Convergence Zone (ITCZ). The clear areas in the central and eastern Pacific are weaker but cover a very large area parallelling the ITCZ. The convergence off the West coast of South America is stronger than any other season. The inferred convection in the EBBI field is less intense than JJA but more centralized over Venezuela feeding the upper-tropospheric convergence zone off the coast.

The onset of the cold season over Siberia forces the surface winds we discussed in JJA to reverse direction from 'southerlies' to 'northerlies'. This increases the convergence into the PMC and signals the start of the winter monsoon season. Over Africa the EBBI pattern shows the western convective cell moves off-shore to the central Atlantic. The divergent winds sup-

port the inferred convection and subsidence in the EBBI field over central and northern Africa.

We compared the patterns of Figures 1-8 with the January, April, July, and October figures in Arkin et. al. (1986) which was a similar study of monthly mean velocity potentials from October 1978 to September 1983. The velocity potential distributions are identical except for sign. We use the convention that irrotational wind blows from High velocity potentials to low velocity potentials, Arkin et. al. use the opposite convention.

Several characteristics of the intra-annual cycle appear in these figures. The first is the dominance of the PMC divergence center in governing the global Hadley regime. Second is the seasonal variation in the location and intensity of this center in alignment with the winter and summer monsoons. It is evident from the horizontal irrotational wind field that this western Pacific High is the source for the tropical Hadley branch of the general circulation. As we shall see in the next section, the seasonal variation of the Hadley cell is dominated by the seasonal north-south movement of this convection.

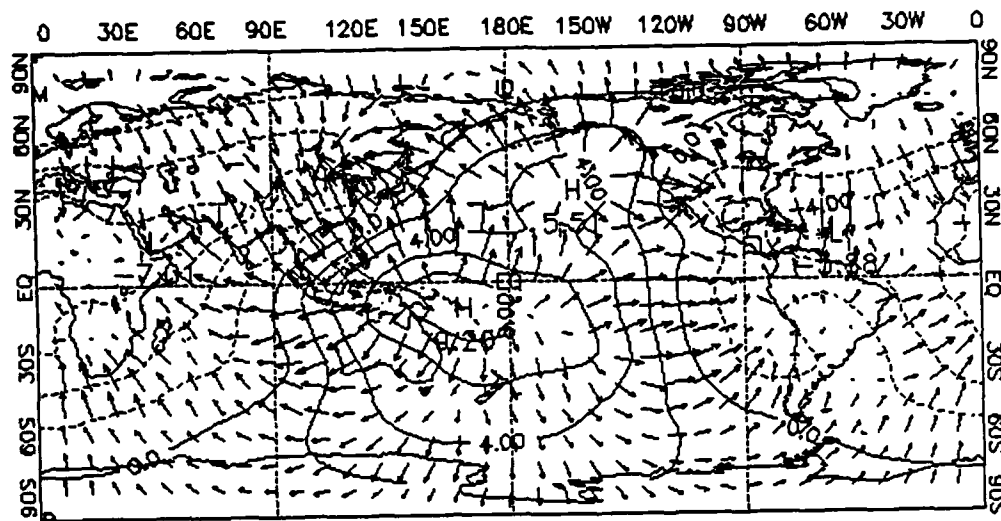
The 200 mb PMC outflow is stronger to the west than to the east. We also observed differences in hemispheric patterns. Some of these differences are related to the zonally asymmetric distribution of land/sea mass about the equator. The southern hemisphere (SH) patterns are more persistent because of the stable heating gradients associated with its large water mass. In the northern hemisphere, large land masses contribute to heating differentials between the land/sea topography. This causes substantial

fluctuations in the circulations.

The patterns in the southern hemisphere show only the slightest variations but magnitudes do vary between seasons. The western flow from the PMC source converges into the upper-tropospheric sink off the east African coast and the eastern flow converges into the SPCZ sink. These 'westerlies' reorganize off the east coast of South America and converge into the sink off the southwest coast of Africa.

The EBBI pattern infers a continuous convective belt see-sawing along the equator which is associated with the seasonal changes. Clear sky returns bound this convective band to the north and south. The dominant convection is in the vicinity of the PMC but varies according to the monsoon activity in this area. The most intense activity is during the summer monsoon when convection spreads from the PMC to the Indian subcontinent. This variation in intensity parallels changes in the intensity of the 200 mb irrotational wind field. From a qualitative view, it appears velocity potential and OLR data agree on the inferred spatial placement of upper-tropospheric tropical divergence and convergence centers.

(1a) Mean Velocity Potential & Irrotational Velocity Vectors



(1b) Mean OLRI

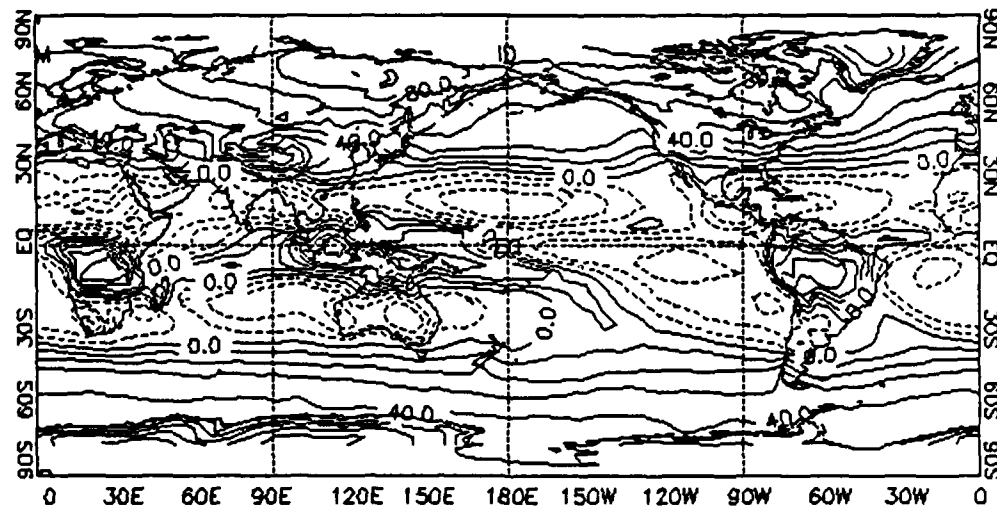
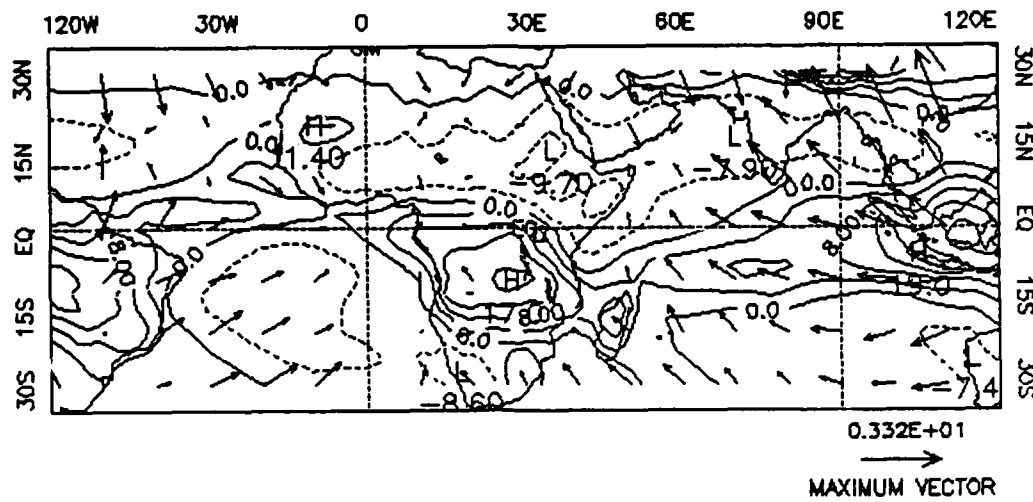


Figure 1. DJF, (a) Mean 200 mb velocity potential and irrotational velocity vectors., contour interval $2 \times 10^6 \text{ m}^2 \text{ s}^{-2}$. (b) OLRI, contour interval 10 w m^{-2} .

(2a) Mean EBBI & Irrotational Velocity Vectors



(2b)

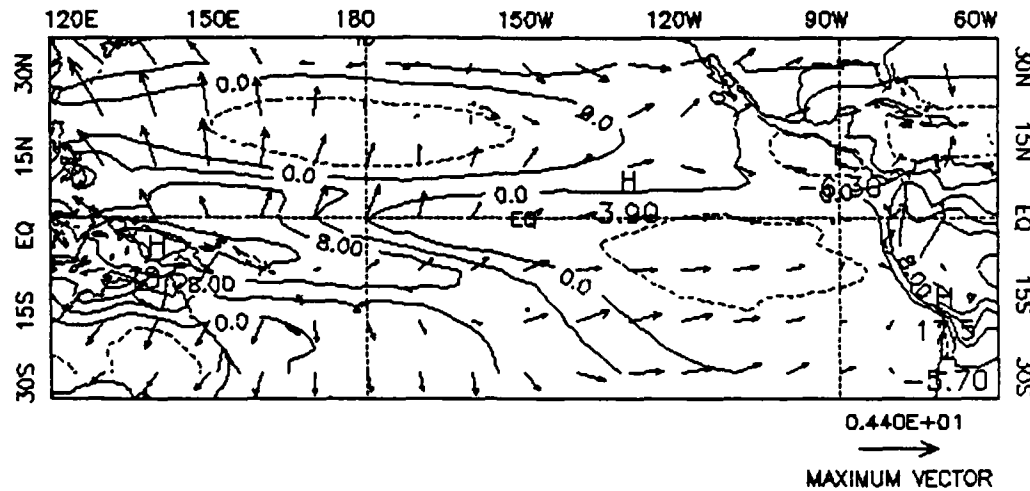
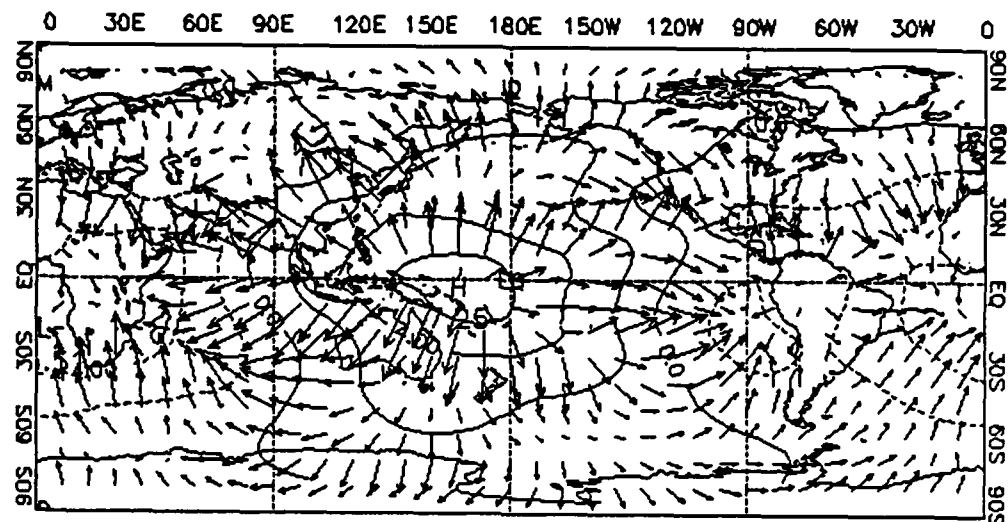


Figure 2. DJF, Mean EBBI ($^{\circ}\text{K}$) with superposed irrotational velocity vectors (m/s), EBBI contour interval 4°K .

(3a) Mean Velocity Potential & Irrotational Velocity Vectors



(3b) Mean OLRI

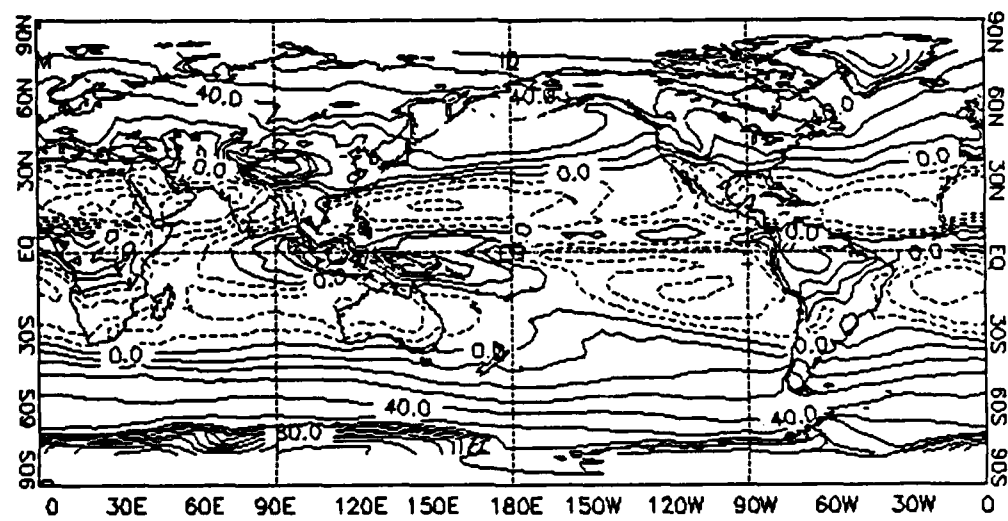
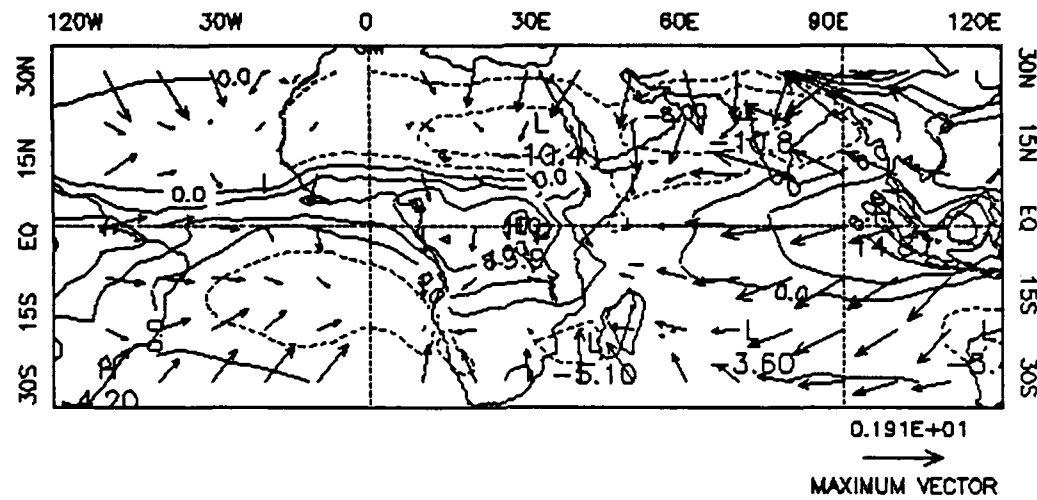


Figure 3. As in Fig 1 except for MAM.

(4a) Mean EBBI & Irrotational Velocity Vectors



(4b)

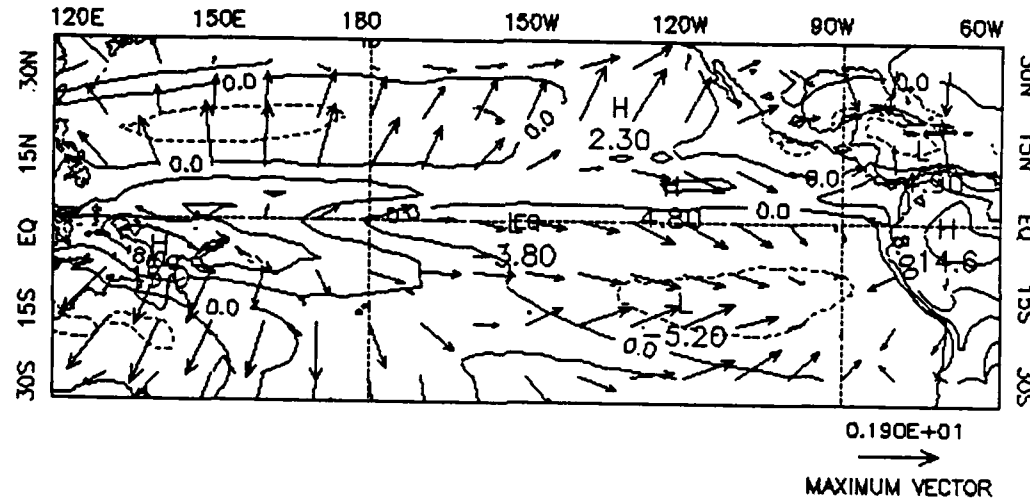
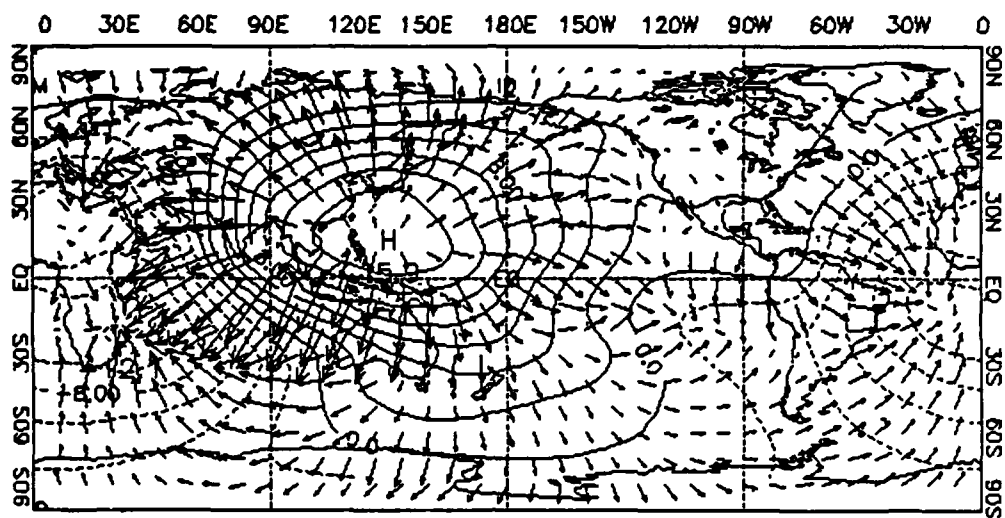


Figure 4. As in Figure 2 except for MAM.

(5a) Mean Velocity Potential & Irrotational Velocity Vectors



(5b) Mean OLRI

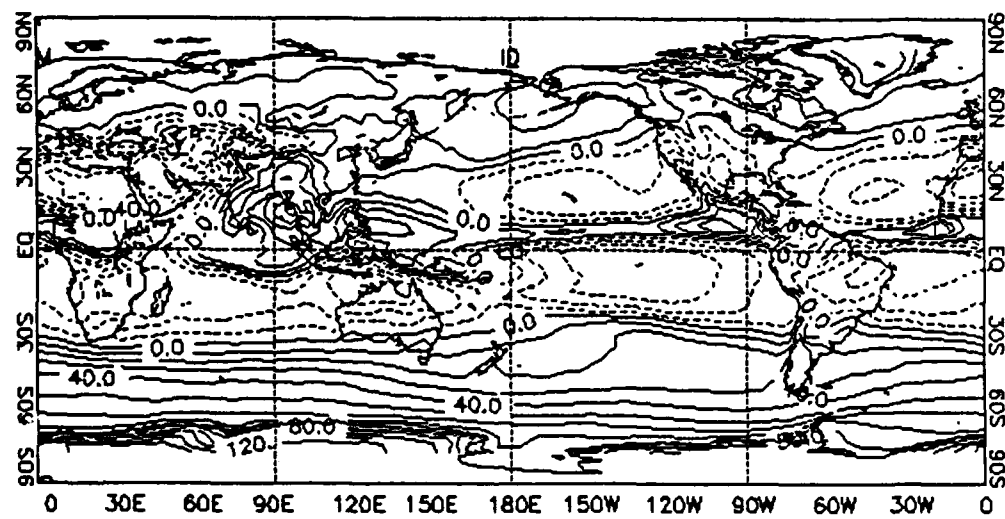
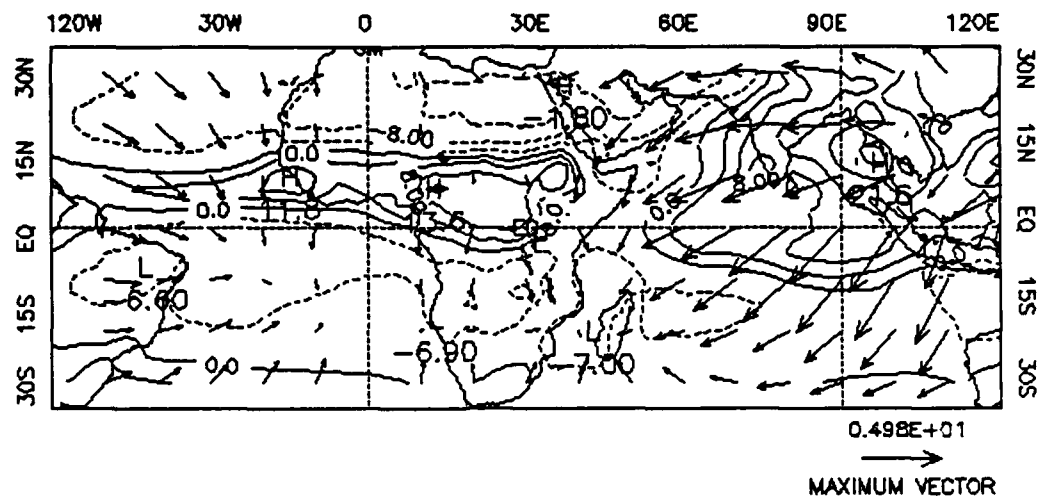


Figure 5. As in Figure 1 except for JJA.

(6a) Mean EBBI & Irrotational Velocity Vectors



(6b)

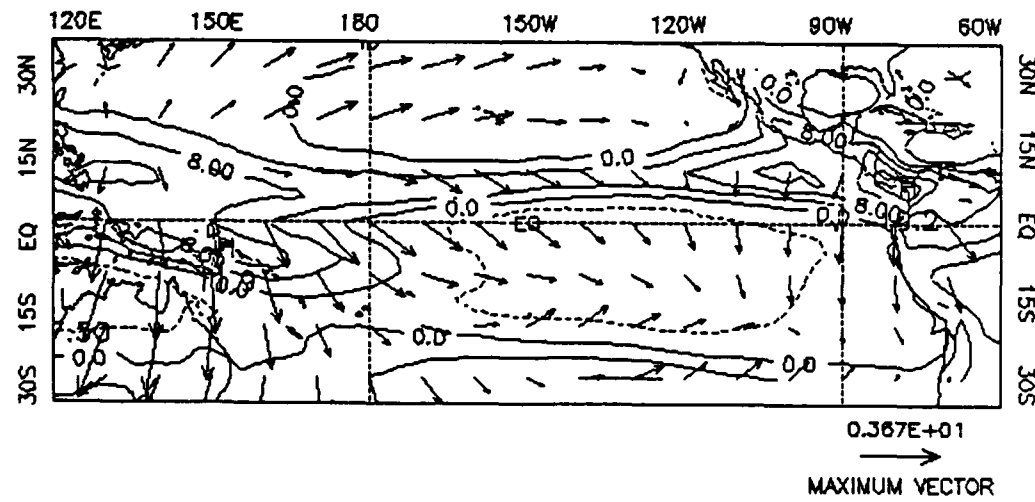
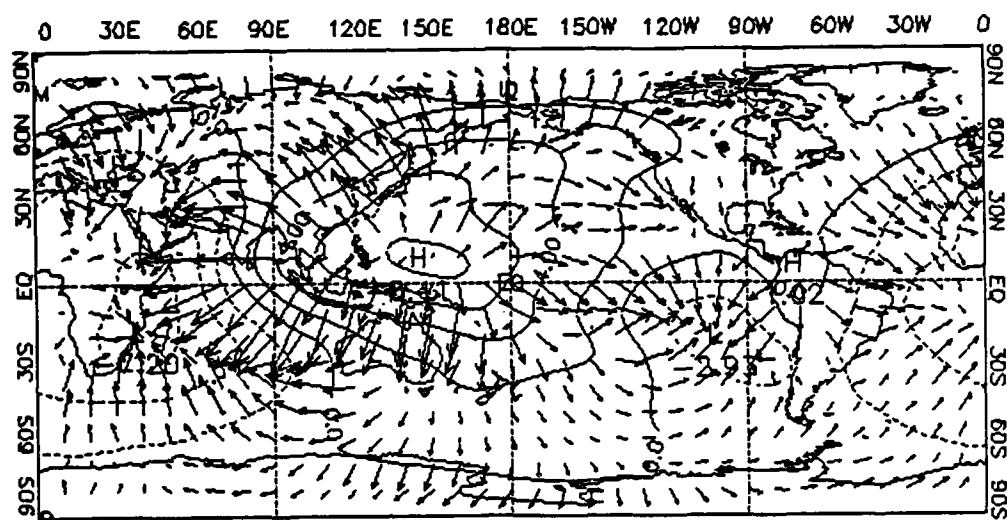


Figure 6. As in Figure 2 except for JJA.

(7a) Mean Velocity Potential & Irrotational Velocity Vectors



(7b) Mean OLRI

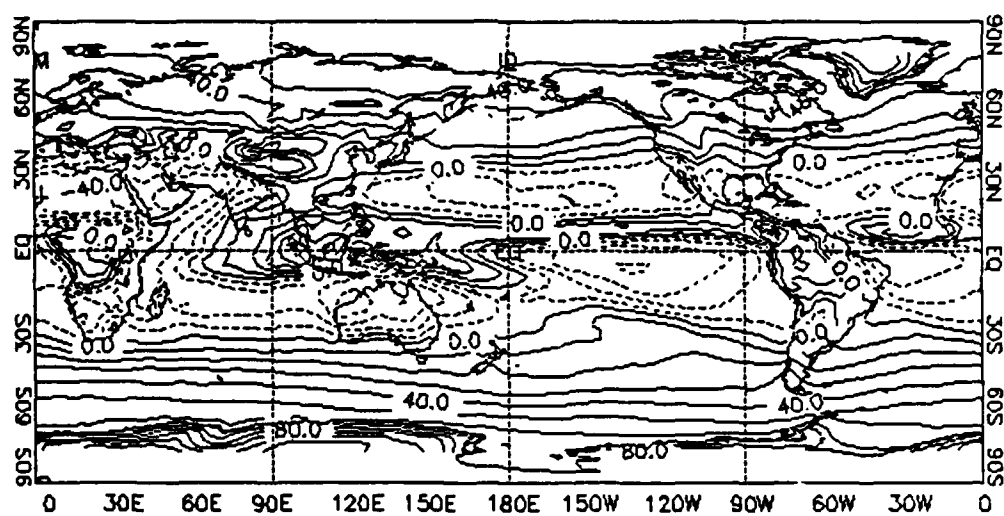
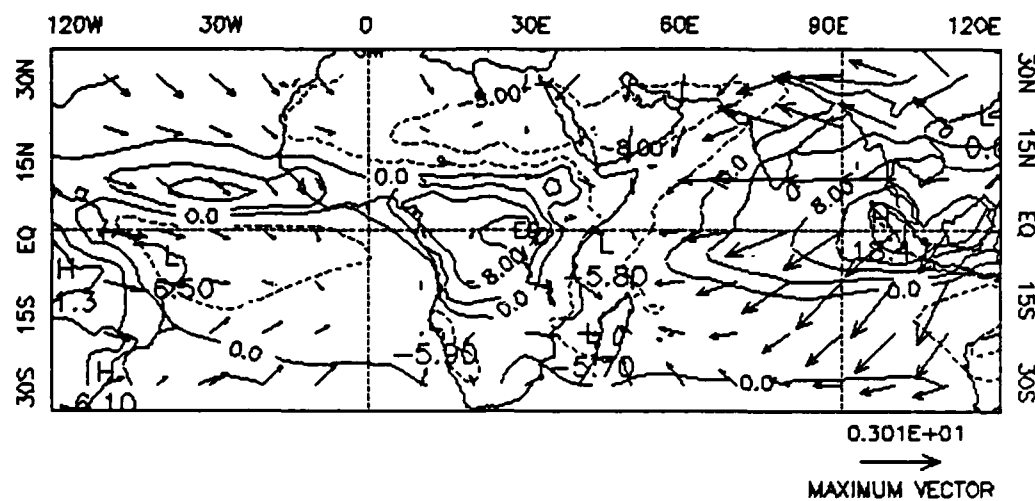


Figure 7. As in Figure 1 except for SON.

(8a) Mean EBBI & Irrotational Velocity Vectors



(8b)

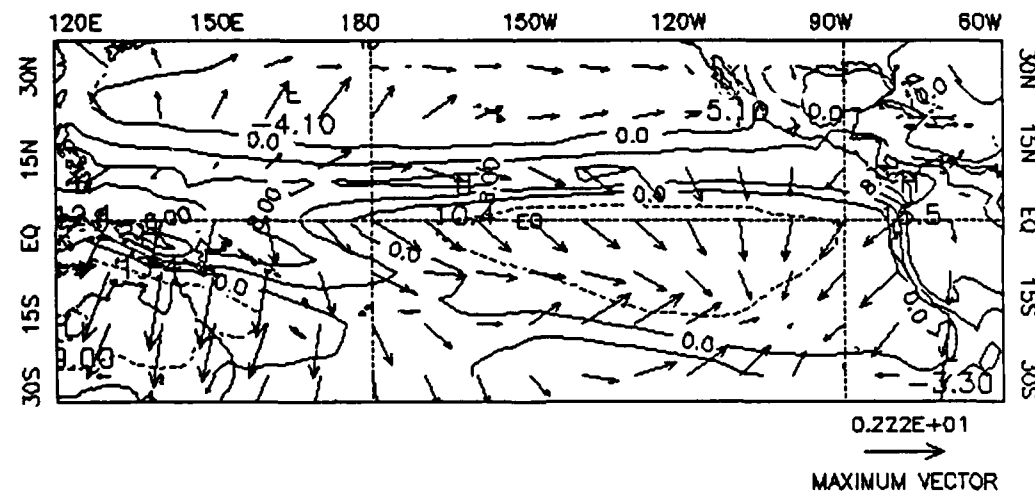


Figure 8. As in Figure 2 except for SON.

4. Mean Meridional Circulation

In Chapter 3 we showed the seasonal variations of the velocity potential field and the 200 mb divergent circulation associated with overturning motions in the meridional and zonal planes. In this section we look at the intra- and inter-annual variations of zonal mean meridional velocity, 200 mb divergence, and zonal mean EBBI.

Figure 9a shows the intra-annual variations of zonal mean meridional velocity. The positive (negative) values represent northerly (southerly) flow. The arrows which have been superposed on some of these figures are meant to highlight the inferred direction of the flow and are not related to their intensities.

The zero contour near the equator in Figure 9a is the 200 mb divergence line which represents the ascending branch of the equatorial Hadley cell. During DJF this branch is found at 20° S and the inter-hemisphere flow is directed from the southern hemisphere (SH) to the northern hemisphere (NH). This pattern reverses by JJA when the ascending branch is found at 30° N and the inter-hemisphere flow is now from NH to SH. The descending branches of the equatorial Hadley cell are near 30° N and 30° S during DJF. In the SH it remains near 30° S throughout the year but in the NH it is in the vicinity of 50° N in JJA.

Oort and Rasmusson (1970) studied the inter-annual variations of mean meridional circulations based on the 5-year period from May 1958 to April 1963. Our results generally agree with theirs but there are some significant differences. The major difference is that our magnitudes were

considerably smaller than theirs particularly in the northern hemisphere DJF where their values were three times larger than ours. They show the maxima in the JJA ascending branch in August while our maxima occurs in July and is found 10° further south. Another difference is in the NH above 30° N where the lip of northerly flow extending to 35° N during JJA is not found in their results.

Figure 9b is the inter-annual cycle of the zonal mean meridional velocity. The vertical lines superposed on this, and Figure 11a, show the month when analysis changes to the GDAS were implemented. These partitions highlight the major weakness of this data set which is the inhomogeneity over the 8 year period caused by the changes. At the same time, these figures support the assumption stated in Section 3 that phases remain constant through the data changes.

The figure shows a strong cellular cycle in the tropical belt from 30° N to 30° S where northerly winds are replaced by southerly winds with 6 month period. This periodicity is associated with the seasonal fluctuations of the equatorial Hadley cell. This cycle remains both spatially and temporally consistent over the 8 years with maximum southerly winds at 10° N during DJF and maximum northerly winds at 5° S during JJA. The only variations are in the magnitudes, particularly in 1986 after the last GDAS changes were implemented. In JJA of 1986 the northerly wind has a magnitude of -4.25 m/s, compared to values in the range of 1.9 m/s to 1.6 m/s from 1980 to 1984. In spite of magnitude variations, the annual cycle remains very consistent over the entire 8 years.

The oscillations north of 30° N are the variations associated with the NH Ferrel cell. This cell shows similar oscillations to those of the equatorial Hadley cell but the SH Ferrel observed south of 30° S shows hardly any variations. The one exception is during DJF of 1983 and 1984 when the northward flow pattern extends across 20° S bridging through to the descending motions of the SH Ferrel cell at 30° S. In the divergence, as we will see, there is also some discontinuity during these periods. These variations are possibly related to the 1982-83 El Nino event.

Figure 10a shows the intra-annual cycle of the mean zonal divergence and 10b the mean zonal EBBI field. We have marked the maxima in to show lines of divergence and convergence. Maxima in equatorial divergence begin at 10° S ... January and moves to 10° N by May. It remains here until November before moving back to 10° S. The SH convergence line varies slightly from 35° S in january to 25° S in July. The NH convergence maxima line appears near 30° N in January and remains there through June.

The mean zonal EBBI field (10b) generally agrees with the divergence field. The line of inferred convection at 10° S in January moves to 5° N by May and then back to 10° S by December. The clear skies in the NH pattern is represented along a line starting at 10° N in January, moves to 20° N by May, then back to 10° N by December. This pattern of equatorial convection, undergoing seasonal cross-equatorial transitions, is found in all of the figures.

Figure 11 shows a comparison between the mean zonal divergence and

the EBBI field. The divergence has a High-Low cellular structure across the equator throughout the 8 years. This pattern is in phase with annual seasonal variations. Large magnitude are again observed after the last GDAS change in 1986 was implemented. In this figure a maximum infers upper-tropospheric horizontal divergence.

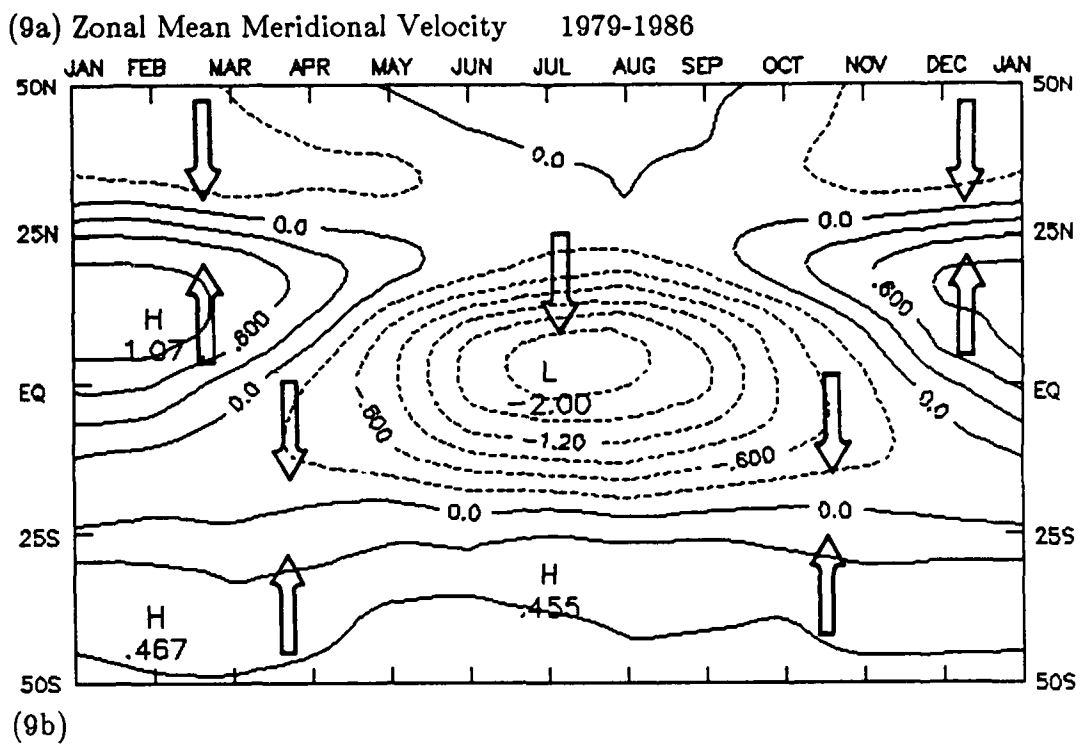
The clearest association between these fields is the wavy pattern along the equator between 20° N to 20° S over the full 8 year cycle. The EBBI pattern is more regular in appearance and maintains its' shape over the 8 years. The divergence field has a slightly jagged appearance with slight breaks in the SH pattern during DJF of 1983 and 1984. This was the same type of variation we observed in the meridional pattern (9b).

These figures infer bands of convergence (11a) and clear skies (11b) between 15° N and 40° N in the NH and 5° S and 30° S in the SH. This implied subsidence region borders the divergence wave. The only disparity is in the NH of 11a where branches of divergence extend across the NH band during JJA.

In this section we observed the intra- and inter-annual variability in the zonal mean meridional velocity, zonal mean divergence, and mean EBBI field. The same general patterns were supported in the divergence and the EBBI field which implies that preferred spatial and temporal zones of 200 mb divergence are supported by two independent data sets. The seasonal meridional transition that was so prevalent in Chapter 3, was supported by both intra- and inter-annual fields. These patterns support the global structure of the tropical Hadley circulation and its characteristic of cross-

equatorial flow patterns. Oort and Rasmusson (1970) showed similar patterns but some discrepancies, especially in magnitudes, were found and attributed to data source considerations.

The inter-annual patterns showed a cellular structure that remains in phase through all the analysis changes. The EBBI pattern was in agreement with the wave-like equatorial pattern we observed in the divergence field. Magnitude variations were most apparent after implementation of GDAS changes in May of 1986. The patterns in the EBBI field and magnitudes over the 8 year period were very stable which is indicative of a homogeneous data set.



(9b)

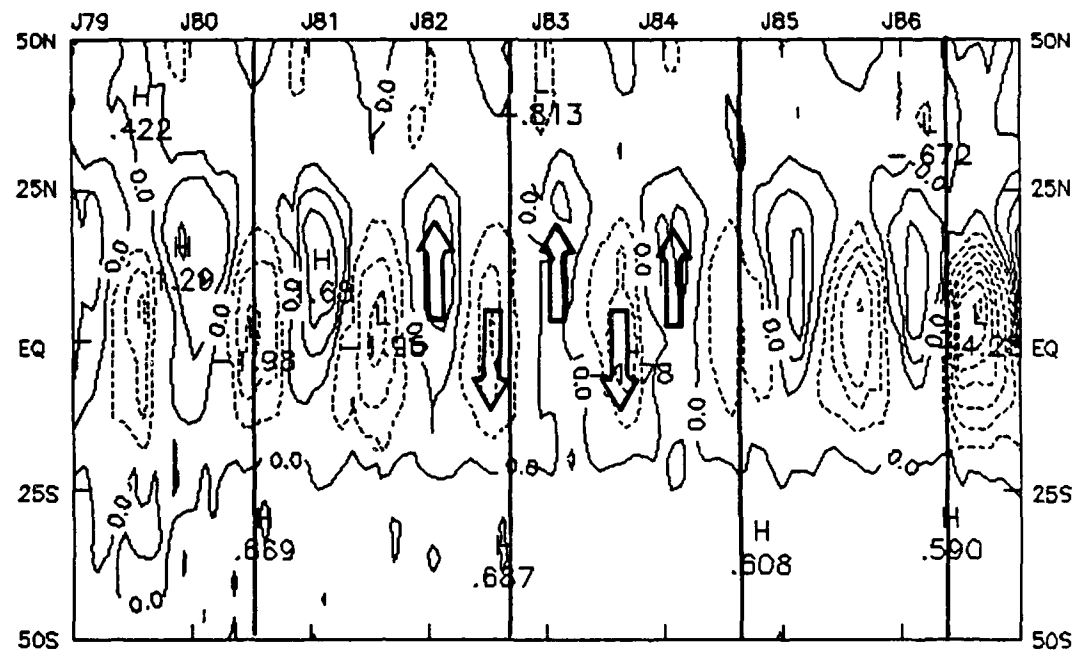
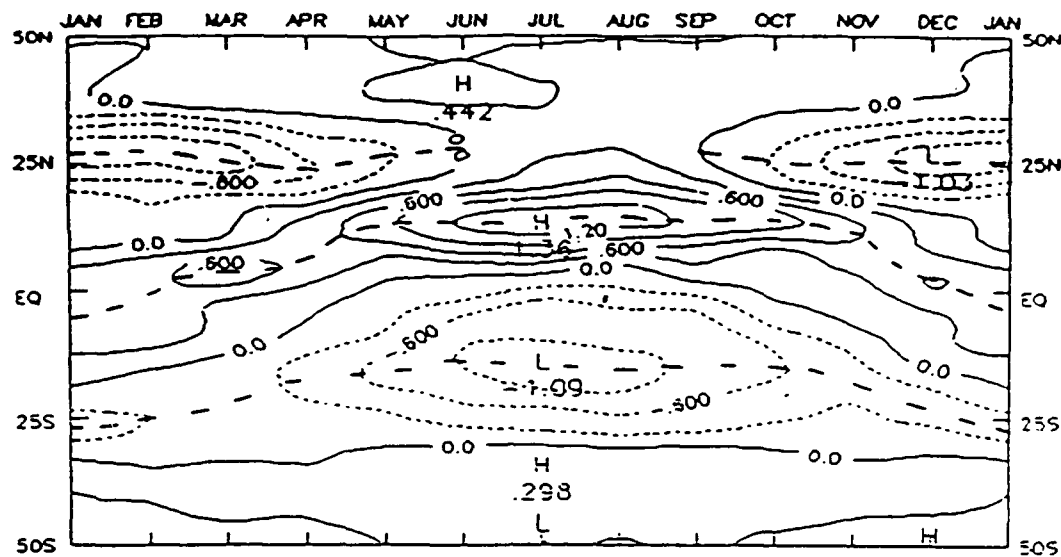


Figure 9. 200 mb zonal mean meridional velocity component, (a) Intra-annual variability, contour interval .3 m/s. (b) Inter-annual variability, contour interval .6 m/s. Vertical lines are times of GDAS changes.

(10a) Zonal Mean Divergence 1979-1986



(10b) Zonal Mean EBBI

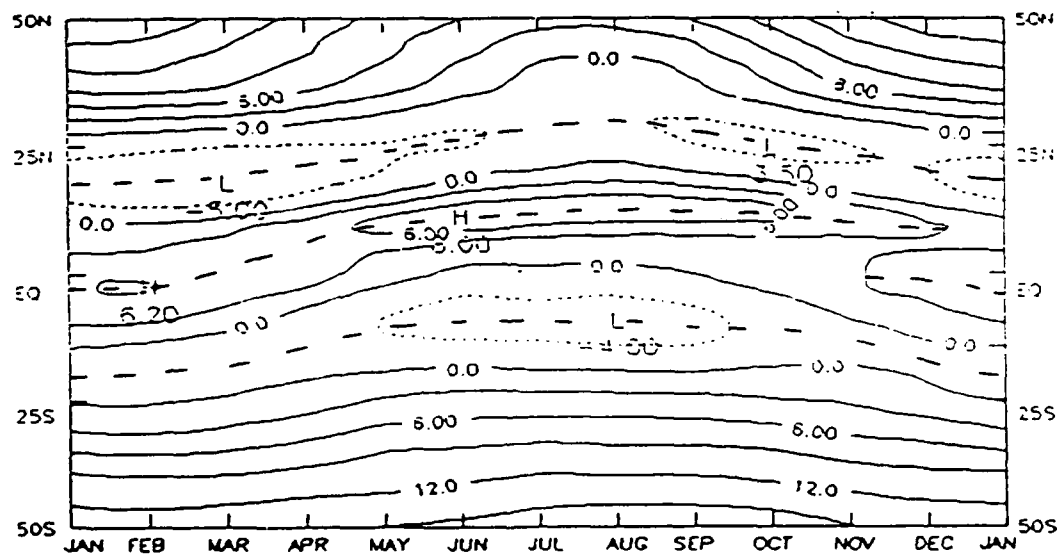
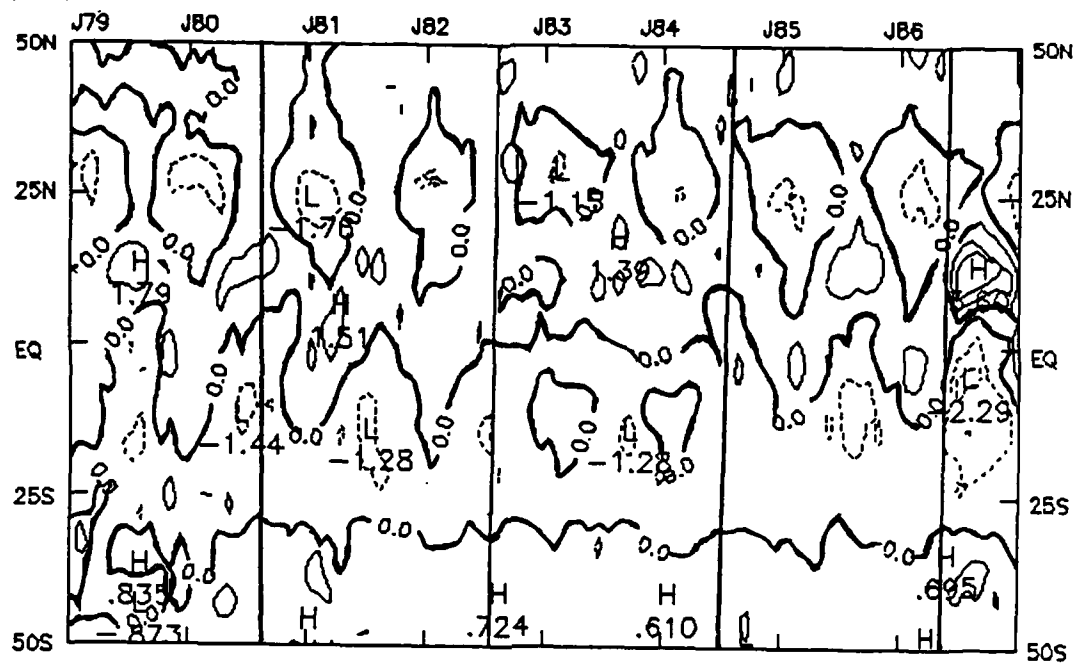


Figure 10. Intra-annual variability, (a) 200 mb zonal mean divergence, contour interval $1 \times 10^{-6} \text{ s}^{-1}$. (b) EBBI, contour interval 3°K .

(11a) Zonal Mean Divergence 1979-1986



(11b) Zonal Mean EBBI

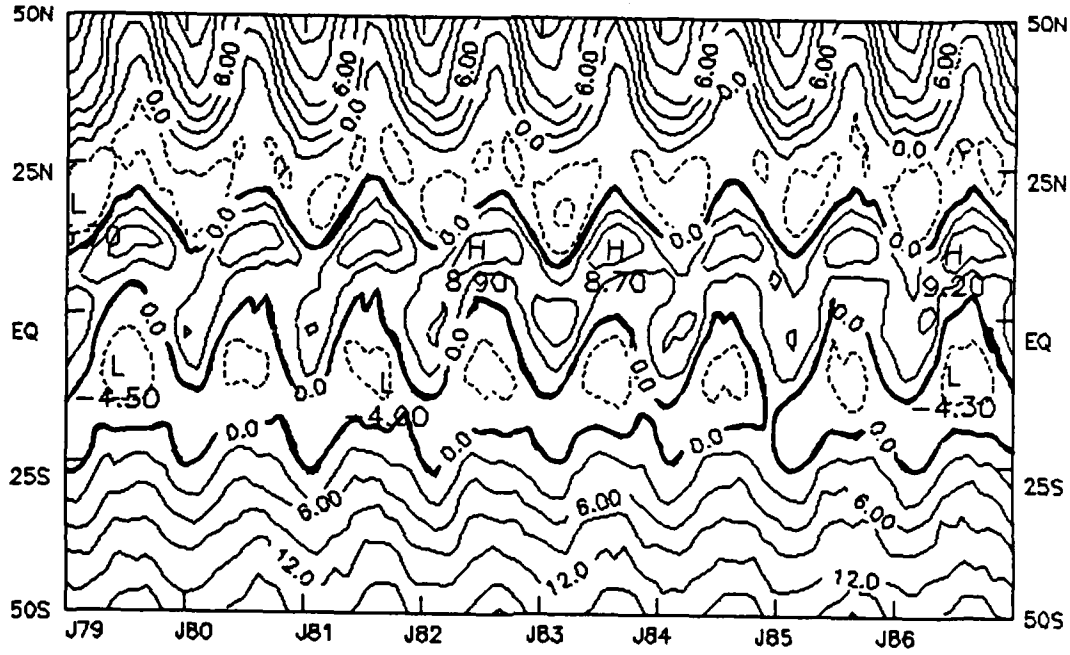


Figure 11. Inter-annual variability, (a) 200 mb zonal mean divergence, contour interval $3 \times 10^{-6} \text{ s}^{-1}$ Vertical lines are times of GDAS changes. (b) EBBI, contour interval 6° K .

5. Mean Zonal Circulations

The Walker cell is a system of zonal overturning motions in the south Pacific which is one component of a broader system of zonal overturning motions in the tropical belt. Its motions ascend in the western monsoon region and descend off the eastern South American coast. Bjerknes (1969) used a small tropical data set to show the existence and describe the structure of this circulation. The timeliness of Bjerknes' work, in conjunction with the increased availability of tropical data, led to several related studies.

Krishnamurti (1971a) studied the tropical east-west circulations using 200 mb velocity potential data from JJA of 1967. In 1973 he collected and analyzed the same variables from DJF of 1969 to complete his description of the seasonal variability in this field. He observed that 200 mb east-west overturning motions came from the same monsoon region described by Bjerknes in 1969 and described it as a southern extension of the main east-west flow pattern about the equator.

Our analysis confirmed Krishnamurti's observations that the Asian monsoons are the center for global divergent motions. In addition, the east-west overturning motions over the Atlantic were strongly influenced by convection over South America during each of the seasons. The isopleths in JJA (figure 5) showed comparable magnitudes between Hadley and east-west motions. Krishnamurti measured the intensity of east-west circulations by calculating (I_E):

$$I_E(\chi) = - \frac{1}{y_2 - y_1} \sum_{i=y_1}^{y_2} \frac{\partial \chi_i}{\partial x} dy \quad (12)$$

where y_1 and y_2 are the southern and northern limits of the belt and I_E varies along x . We chose the same latitude belts used by Krishnamurti: in DJF y_1 and y_2 are $15^\circ S$ and $15^\circ N$ and in JJA they are $0^\circ N$ and $30^\circ N$ respectively.

Figure 12 shows the mean zonal divergent winds for the two major convective latitude belts described above. Positive (negative) values are eastward- (westward-) directed 200 mb irrotational velocities. The magnitudes appear to be very even between the two seasons but the positions of the circulations shift to the west by about 60° from DJF to JJA. The easterlies are associated with an anti-clockwise cell in the vertical plane with a rising branch over the monsoon region and a descending branch over Africa. The westerlies over the Pacific Ocean are associated with the so called Walker circulation.

These observations agreed with the spatial patterns in Krishnamurti's figures except for slightly higher magnitudes in our patterns. Because his analysis was based on a very limited number of observations taken over one season, it is highly likely the discrepancies are found in the data sources.

Figure 13a is the monthly mean 200 mb zonal variations of the irrotational velocity field averaged over 8 years and the latitude belt from $15^\circ N$ to $15^\circ S$. The sign convention is the same as above. We have highlighted lines of upper-tropospheric convergence (divergence) found at the junction of Low-High (High-Low) patterns. The annual variations of circulations described for Figure 12 can also be seen in this figure. The 200 mb belt of

the 'westerlies' which form the 200 mb component of the Walker cell in the south-central Pacific. The 200 mb divergence waivers from 130°E to 170°E and from 60°W to 80°W . The central line of 200 mb convergence waivers from 80°W to 110°W . The most significant feature are the variations in the western Pacific source and southeastern Pacific sink regions.

The EBBI and Divergence data appear to be in agreement on the placement of major features, such as lines of convection and upper-tropospheric divergence. We can infer a major center of convection in the EBBI field during JJA at 90°E which is slightly east of the 200 mb divergence line in figure 13a. Similar displacements in other divergence/convergence lines between figures 13a and 13b can also be seen.

Figure 14a displays the inter-annual variations of the mean zonal divergence for the same latitude belt as in Figure 13. The inter-annual pattern remains consistent with the patterns described for the intra-annual cycle with one small anomaly in the EBBI field at 150°E in late 1982 where a minimum in the band of positive values implies strong subsidence. Corresponding to this minimum is a belt of inferred convection from 150°W to 120°W which is a zone which normally implies subsidence. Closer examination of the divergence field shows the same type of anomaly pattern with the observation of a maximum indicating a reversal from the normal easterly flow to a westerly component. Since this corresponds to the area and timing of the 1982-83 El Nino event we looked at this period in more detail.

Figure 15 is similar to figure 12 except it shows the mean zonal flow

over the two most active seasons. The January 1982 and 1983 data are averaged over 15°N to 15°S and the July 1982 and 1983 data are averaged over 0°N to 30°N . The figure only cover the longitudes from the Indian Ocean to the east coast of South America to highlight the Pacific circulation. There is a slight variation in magnitudes between 1982 and 1983 but the most significant contrast is the 60° and 30° lag between Januaries and Julies respectively. These lags imply movement of the western Pacific source region associated with the ascending branch of the Walker cell.

In Figure 16, the January 1982 convection is centered over the PMC with easterly flowing divergent velocity vectors on both sides of the equator with convergence off Baja, Mexico, and the SPCZ off the South American coast. In January 1983, the convection has moved to 165°W with divergent velocity maxima decreasing by 25% from 1982 and the divergent flow in the western Pacific has reversed to flow towards the west.

In Figure 17, The ITCZ in July 1982 is clearly marked between 5°N and 10°N from the PMC to the Baja, Mexico. The western 'source' is centered in the NH at 150°E with a maxima in the EBBI of 17.6° and another maxima of 21.4° is found on the northwest tip of Venezuela. The Walker cell circulation is apparent in the divergent velocity vector field. In July 1983 the western Pacific convection is centered at 120°E and the EBBI maxima over Venezuela has shifted 60° northwest of its 1982 position. The EBBI infers a break in the ITCZ at 130°E .

In summary, the analysis of this data generally agrees with Krishnamurti (1971a/b,1973) who also found stronger velocities in the JJA than

DJF cycle. We observed the seasonal cross-equatorial movement in the monsoon convection which feeds the global and tropical energy systems, and the persistence of the patterns over the 8 year period. We also observed significant variations between January 1982 and January 1983 and between July 1982 and July 1983 data. The 1982 data is prior to the start of the El Nino and the 1983 data is during the warming event.

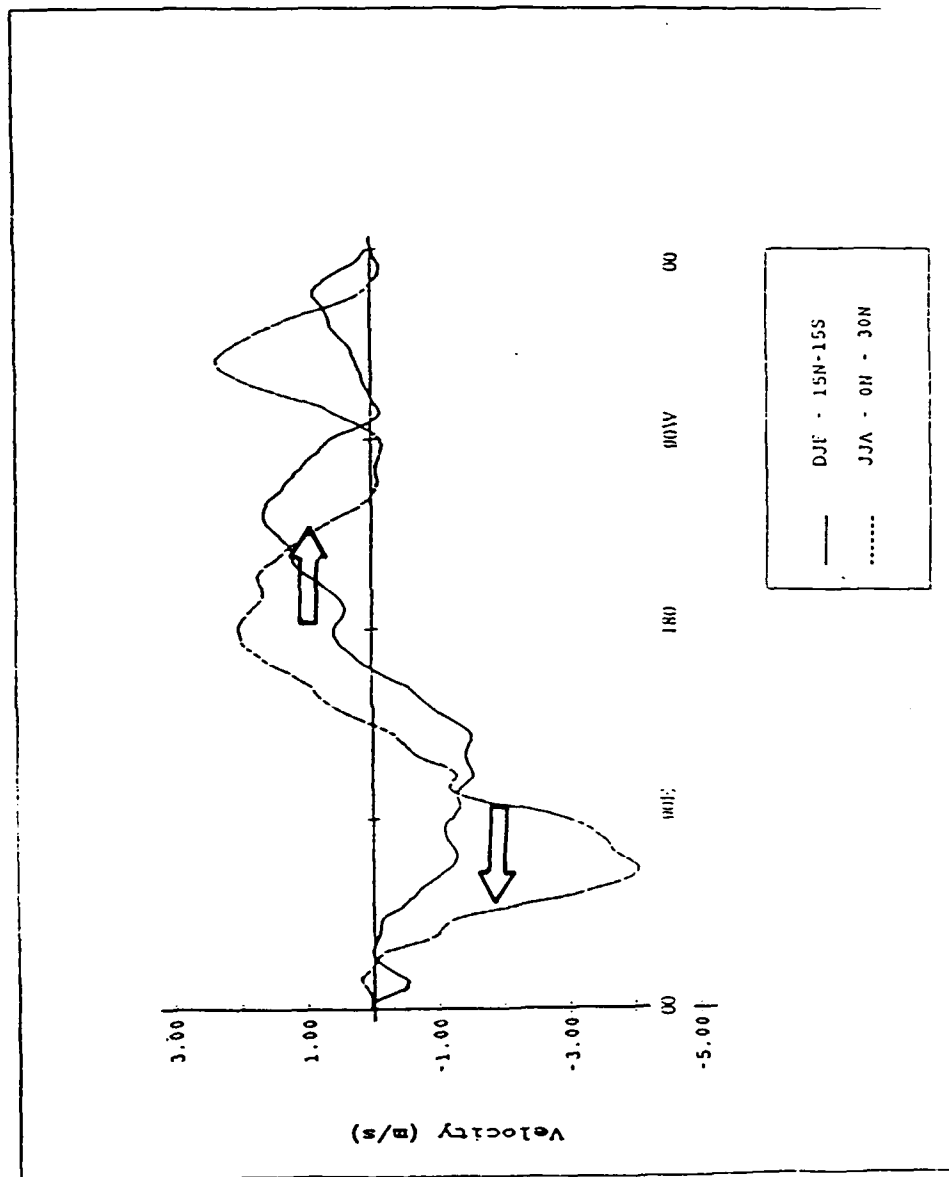
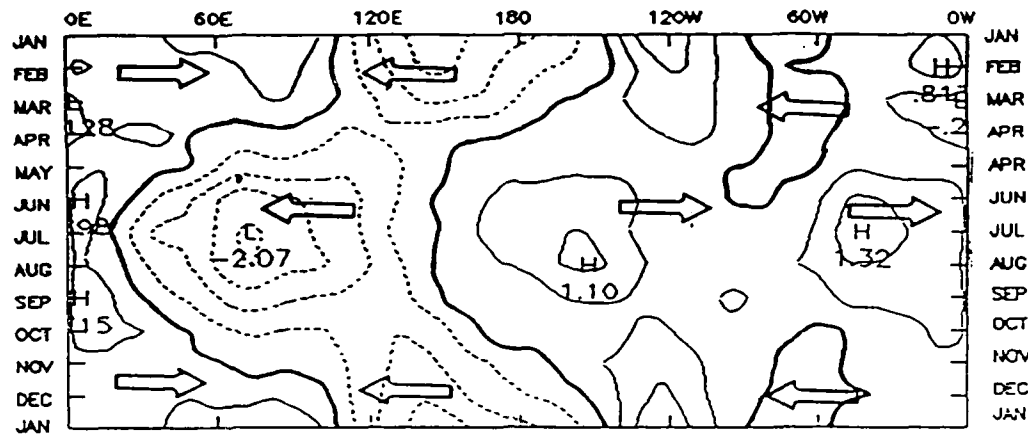


Figure 12. Mean zonal wind averaged over 15° N to 15° S for all DJF's between 1979-1986 and over 0° N to 30° N for all JJA's.

(13a) Zonal Irrotational Velocity Components



(13b) Mean EBBI

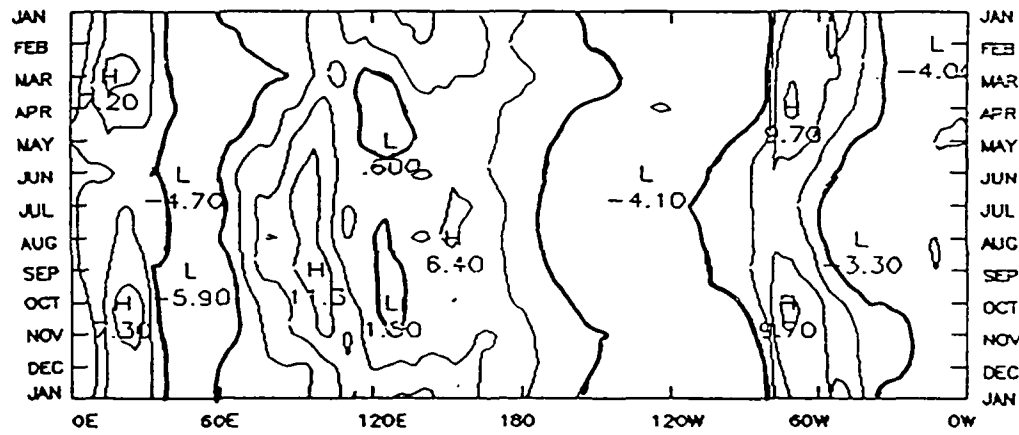
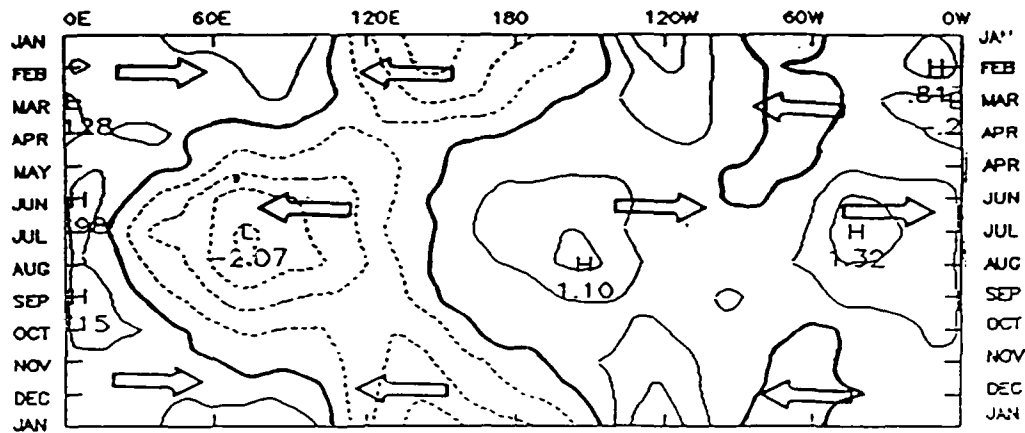


Figure 13. Intra-annual cycle averaged over 15°N to 15°S for (a) zonal irrotational velocity components, contour interval .5 m/s. (b) EBBI, contour interval 3 °K.

(13a) Zonal Irrotational Velocity Components



(13b) Mean EBBI

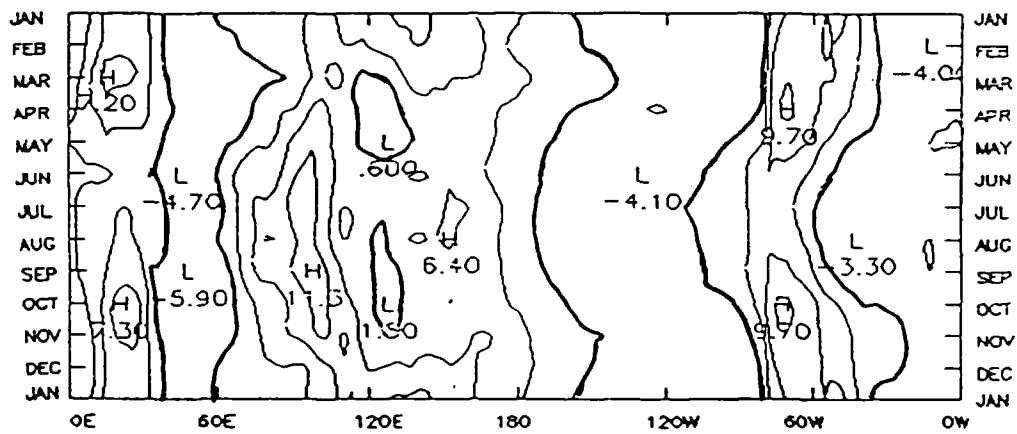
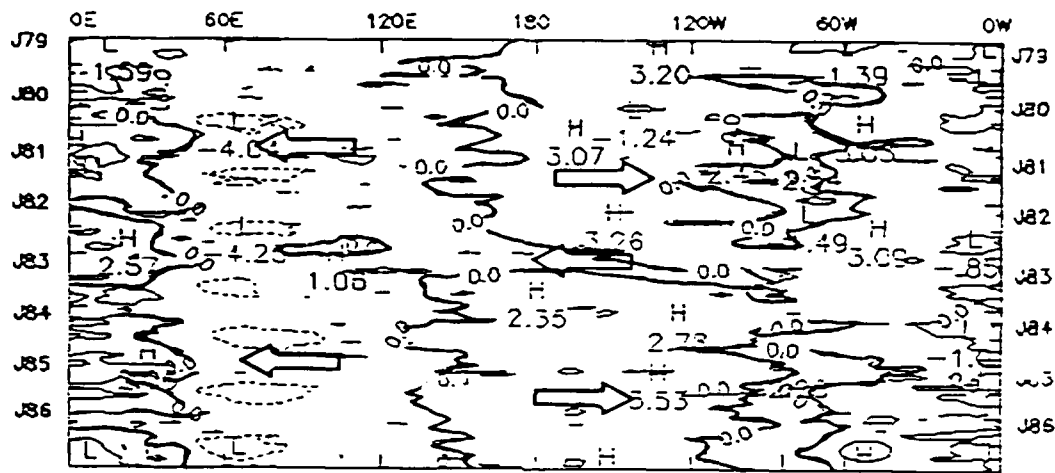


Figure 13. Intra-annual cycle averaged over 15°N to 15°S for (a) zonal irrotational velocity components, contour interval .5 m/s. (b) EBBI, contour interval 3°K.

(14a) Mean Zonal Irrotational Velocity



(14b) Mean OLRI

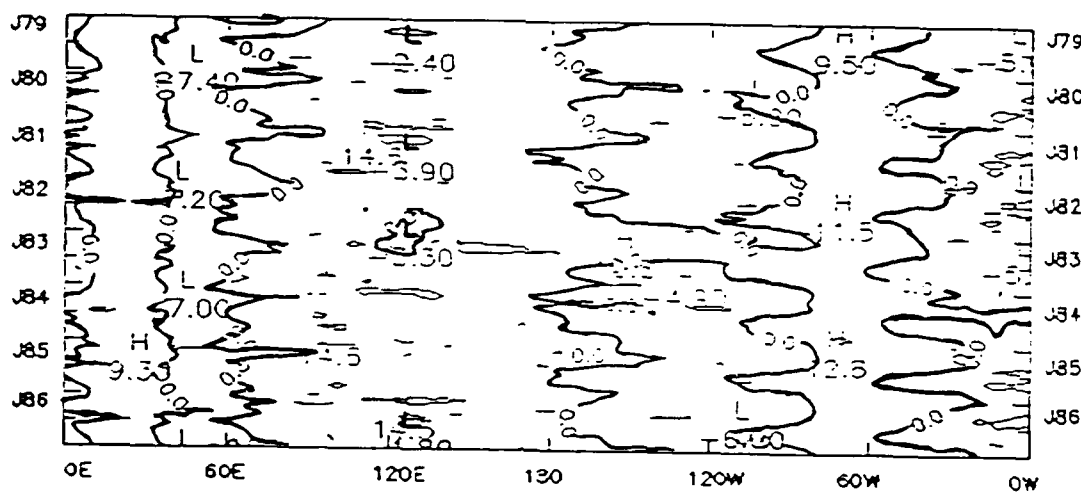


Figure 14. Inter-annual cycle averaged over 15°N to 15°S for (a) zonal irrotational velocity component, contour interval 3 m/s, (b) EBBI, contour interval 10°K .

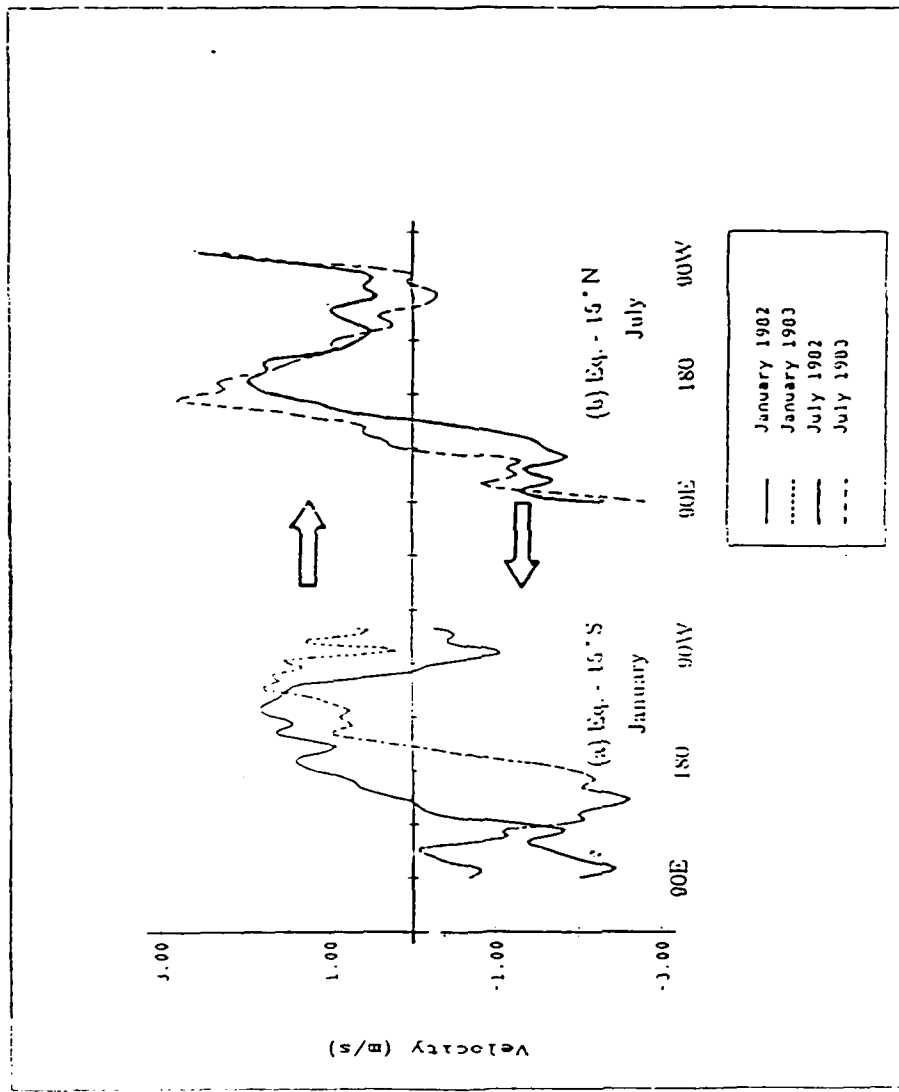
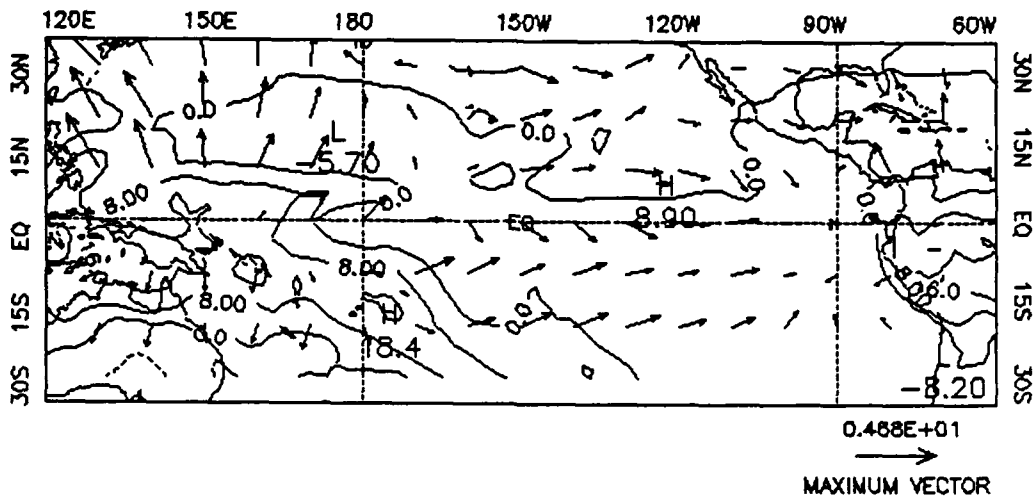


Figure 15. Mean zonal irrotational components 90°E to 60°W . Averages for January (82/83) over 15°N to Eq., and (b) July (82/83) over 15°S to Eq.

(16a) January 1982 120° E to 60° W



(16b) January 1983

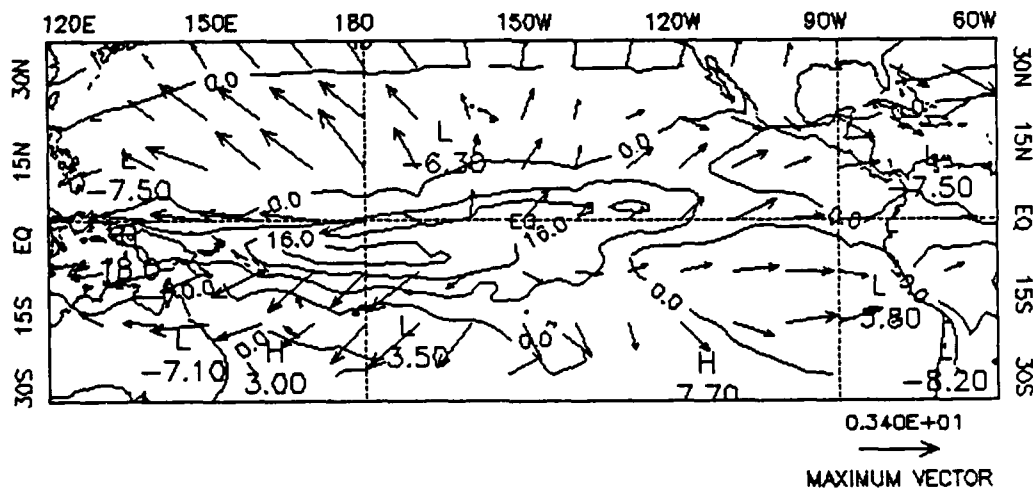
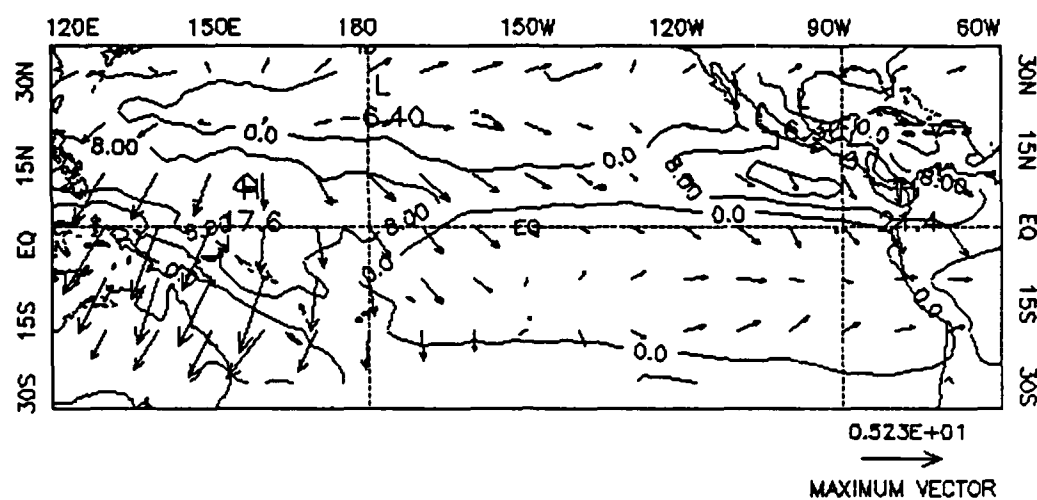


Figure 16. Mean EBBI ($^{\circ}$ K) with superposed irrotational velocity vectors (m/s). EBBI contour interval 8° K.

(17a) July 1982 120° E to 60° W



(17b) July 1983

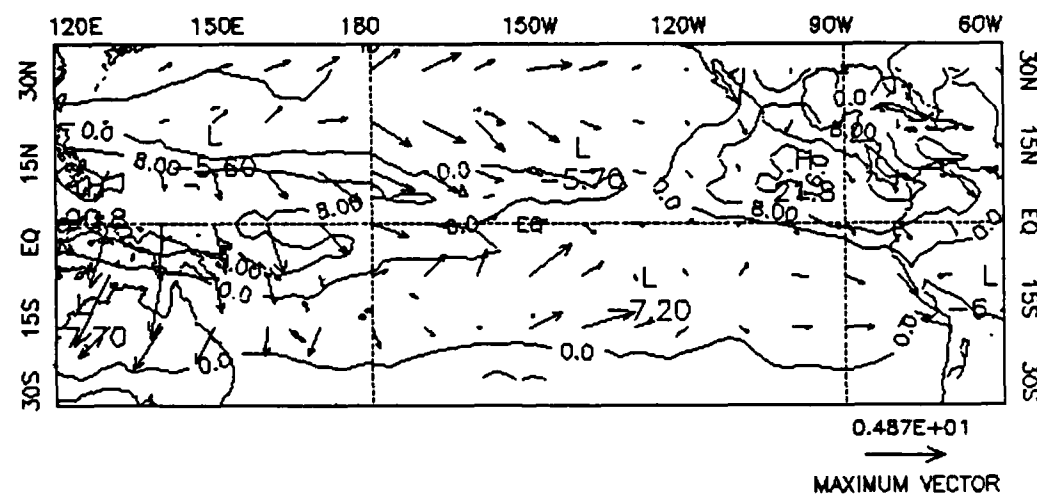


Figure 17. As in Figure 16 except July.

6. 200 mb Divergence and EBBI Correlations

Kasahara (1987b) points out the diabatic NNMI schemes currently used in forecast models underestimate the release of latent heat during the first several hours of the model run and this leads to weakened tropical divergent motions. Different procedures have been studied to improve the accuracy of computing tropical heating rates, including computations from satellite derived data. Richards and Arkin (1981) developed an algorithm for calculating tropical rainfall rates from infrared flux data derived from satellite measurements. They were able to correlate regions of rainfall with low infrared fluxes and latent heat release can then be computed from these rainfall rates. Kasahara et. al. (1987a) also studied this problem using fluxes converted to EBBI fields. They used EBBI as the difference between 260°K and T_e because it is the approximate value of equivalent emission temperature for the earth-atmosphere system. They then correlated this field with the ω field. Their results showed the dividing line between ascending and descending motion is approximately 258°K .

The use of OLR flux as proxy data for conventional observations would partially solve the data gap in tropical latitudes. Convection inferred from OLR flux should be able to provide a gridded divergence field in these latitudes. In order to achieve this, we need to quantify the correlation between the two fields.

Julian (1984) and Kasahara et. al. (1987b) are two examples of ongoing research to accurately quantify the relationship between OLR flux and divergence. They have had some success based on very limited sets of daily

observations. In the present study we use spatial and temporal correlations to our T_E and divergence fields to see if significant correlations are observed over the 8 year data set. The methodology used in computing the different correlations can be found in the Appendix.

Figures 18, 19 and 20 are spatial correlations (Type I) between mean divergence and EBBI fields. The mean values are plotted as a function of longitude, and the correlation between the two fields is indicated in the figure. The correlation in the zone from $5^\circ N$ to the equator is .84 which suggests EBBI explains 70% of the variance of the divergence in the zone whereas the correlation in the $25^\circ N$ to $30^\circ N$ zone is only .26. The overall correlation between the tropical belt between $30^\circ N$ and $30^\circ S$ is .77 explaining about 60% of the variance.

Next we applied temporal correlations (Type II) to January and July fields. The results are shown in Figures 21 to 24 where the .40 and .70 contours of the correlation coefficient are shown. The .70 contour, which is the significant level we determined for this set, is shaded. Accompanying the correlations are the mean EBBI and divergence fields for comparison.

Figures 21 and 22 show similar placements in the inferred divergence centers over South America and the PMC and the same elongated figure to the southeast of the PMC. The EBBI pattern infers divergence extending well west of the PMC into the Indian sub-continent and also over central Africa. Neither of these patterns is found in the divergence patterns. There is some agreement in inferred convergence zones centered at $15^\circ N$ $160^\circ W$, over the Red Sea on the northeast coast of Africa, and in the Caribbean

Sea.

The results on correlations are not as positive as we were expecting. At the significance level computed for the 8 months in the set, there are only small areas of significantly tested correlations between the two sets of data. In the small areas that are correlated, the most significant grouping is in the vicinity of the PMC as we would expect. The central Pacific convergence area described above also shows some good correlations as do other convergence zones off the west coast of South America, and in the Caribbean sea. It is surprising that in these nominal areas, convergence areas are better represented than areas of divergence.

Figures 23 and 24 are similar figures for July. The same dominant divergence centers for this season are again observed. The PMC, the Central American isthmus, and central Africa all reflect strong 200 mb divergence. There is a nice representation of the inter-tropical convergence zone (ITCZ) in the EBBI field that is not as well represented in the divergence field. Only small correlation patterns appear at the significant level and areas of convergence are again as well represented as areas of divergence.

Our objective in this section was to quantify the relationship between OLR flux and the 200 mb divergent circulation. We did this by computing several correlations between our independent data sets. The first correlation of band average mean fields in Figures 18,19, and 20, supported our expectations by returning high correlations in belts of divergence, weak values in belts of convergence, and overall high return for the entire tropical belt. The next set of correlations were disappointing because only isolated patterns of

significant correlations were observed. In all we were successful in showing latitude belts of convection are well correlated with OLR fluxes but were less than successful in finding significant correlations on individual, point-to-point computations. Because these values are needed to make headway in quantifying the relationship between OLR flux and 200 mb divergence we have to say we were not successful.

Band Zonal Average Eq. - 5N Correlation: .84

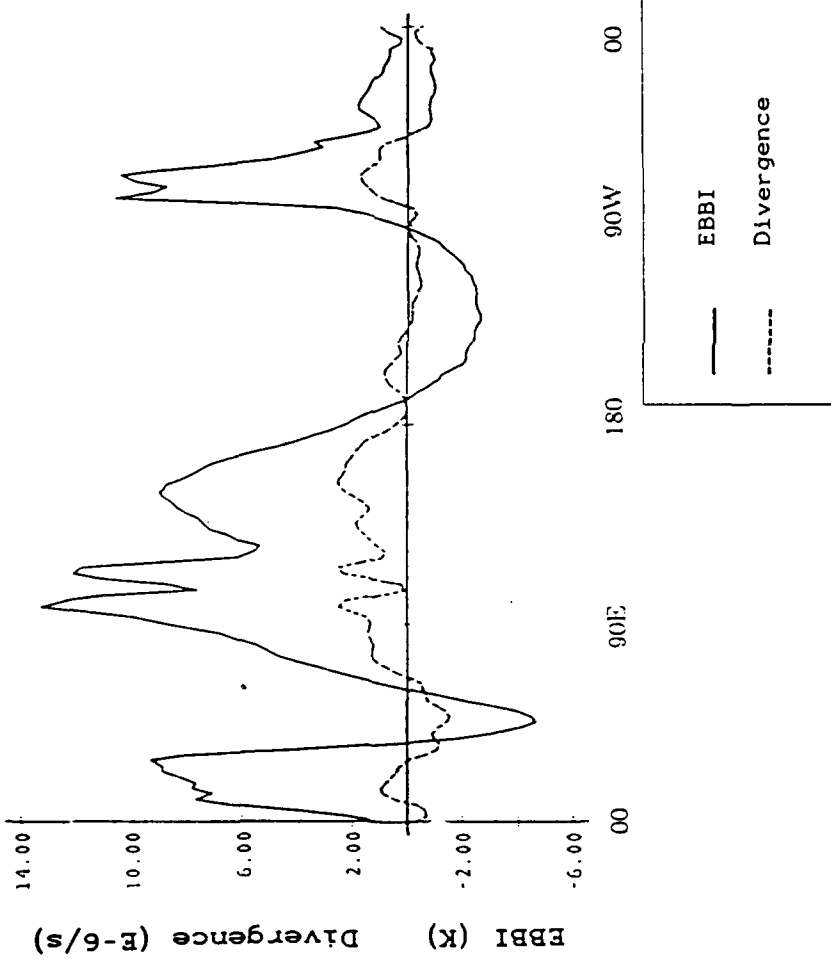


Figure 18. Mean zonal EBBI and Divergence values (scaled by 1×10^5) presented as an 8 year mean, band averaged from 5°N to the Equator.

Band Zonal Average 30N - 25N Correlation: .27

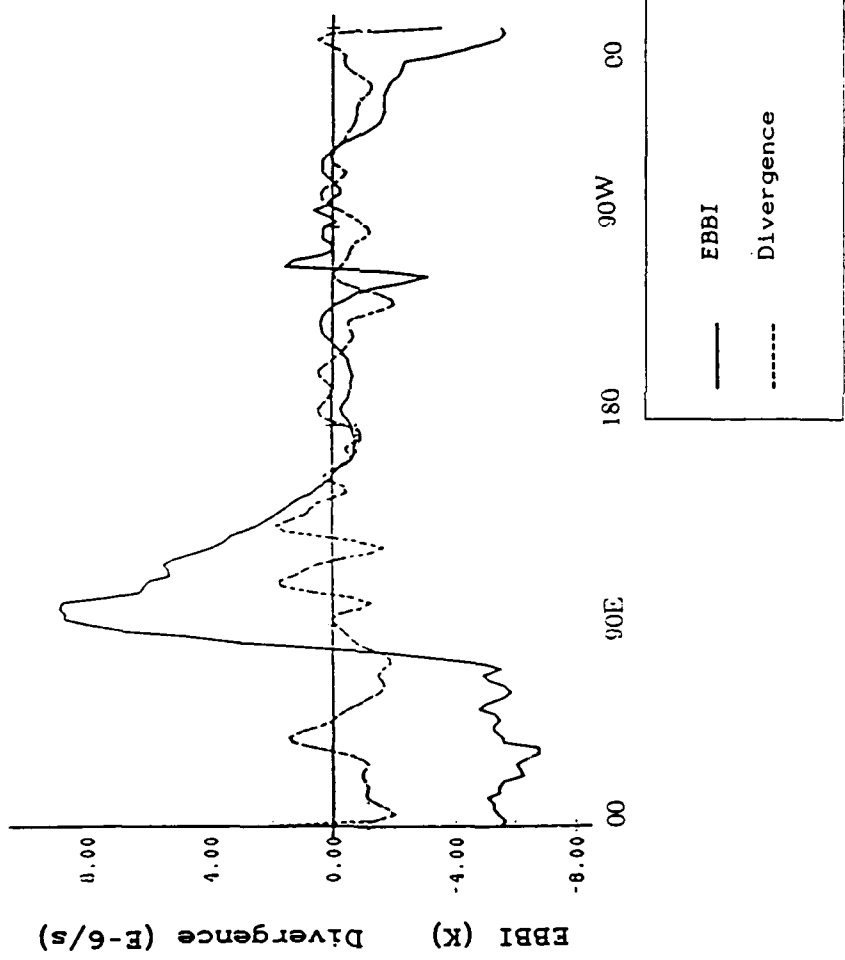


Figure 19. Same as Figure 18 except for the band between 25° N and 30° N.

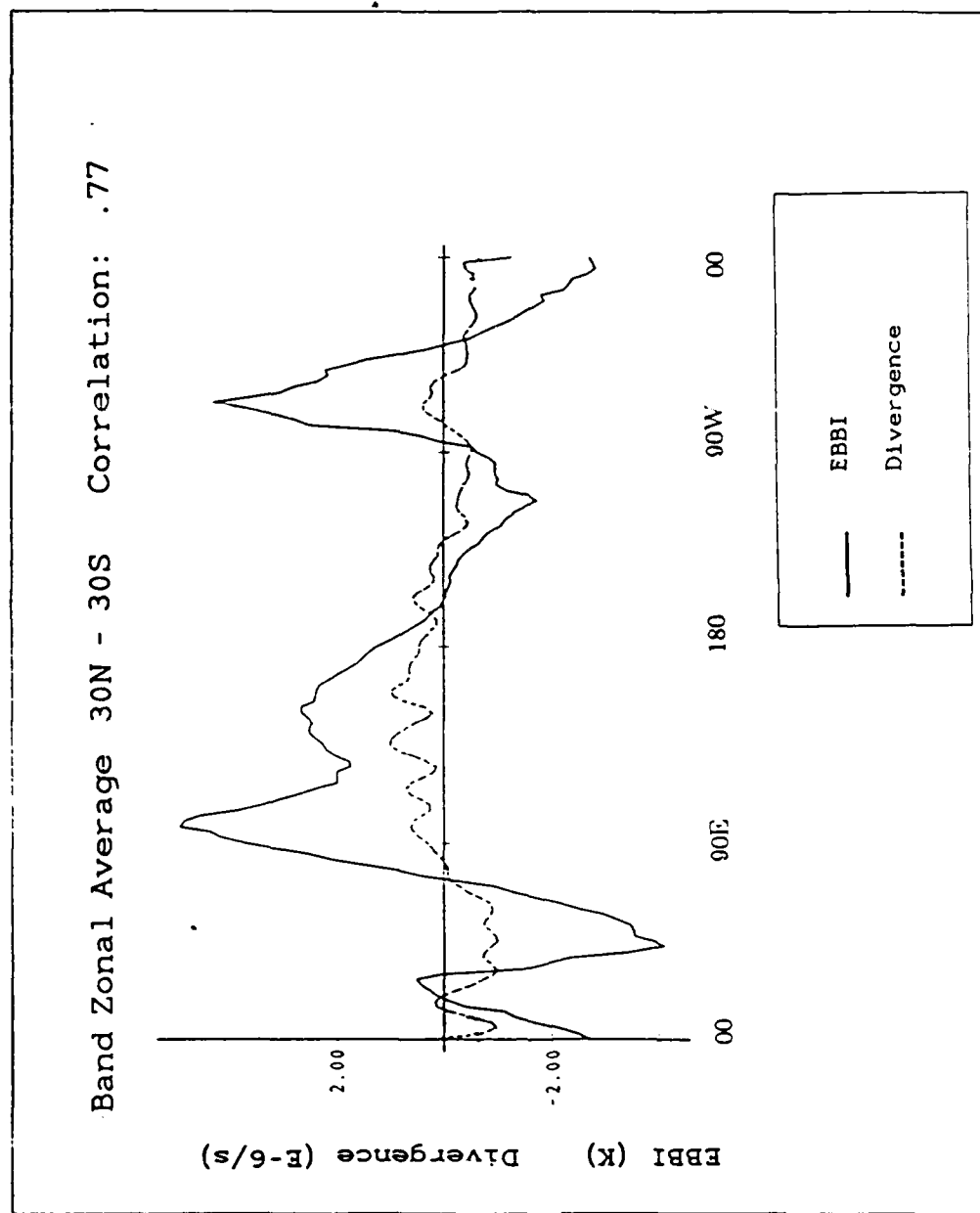
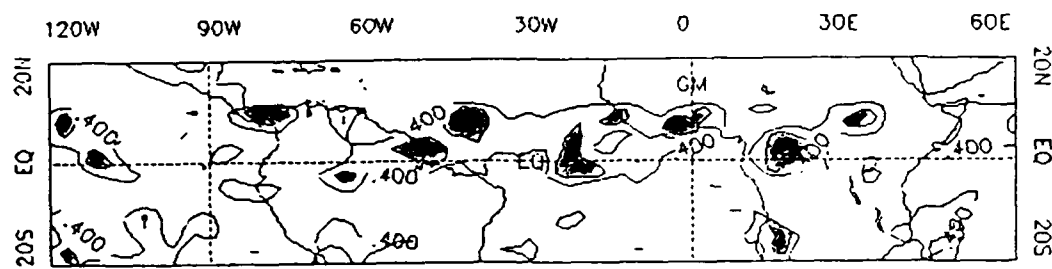
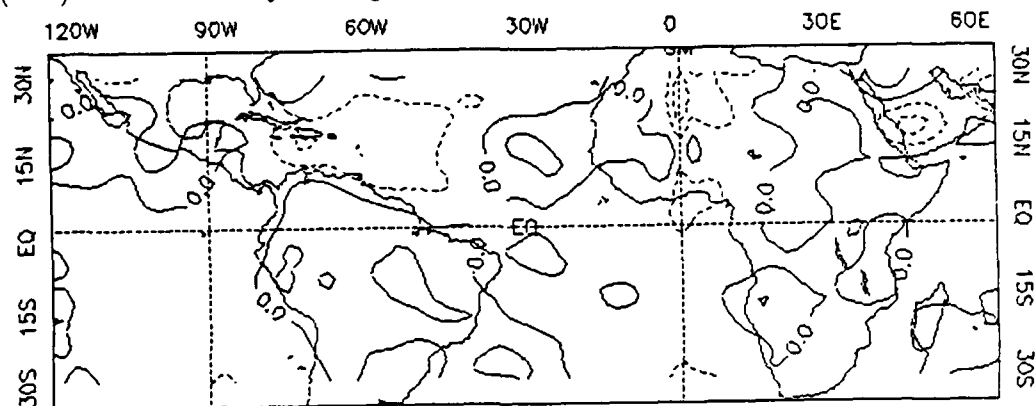


Figure 20. Same as Figure 18 except for the tropical band between 30° N and 30° S.

(21a) Pattern Correlation for January



(21b) Mean January Divergence



(21c) Mean January EBBI

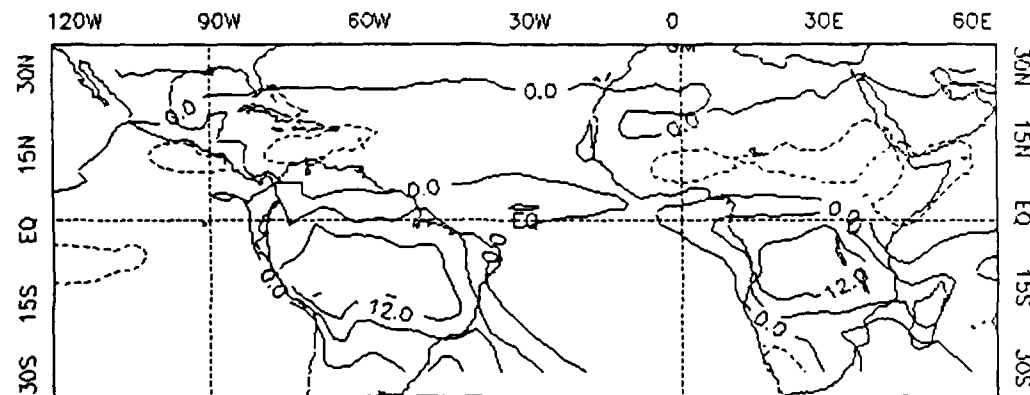
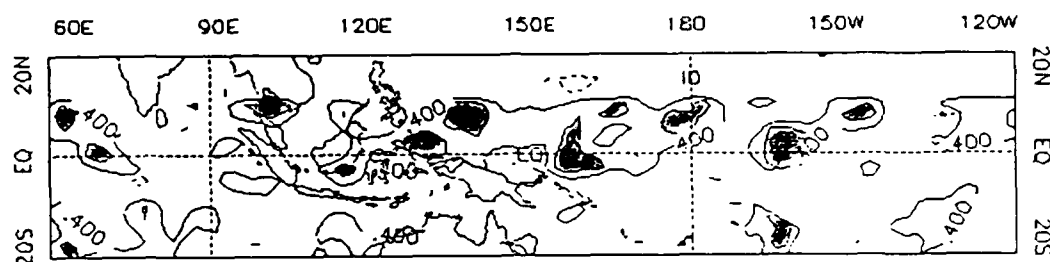
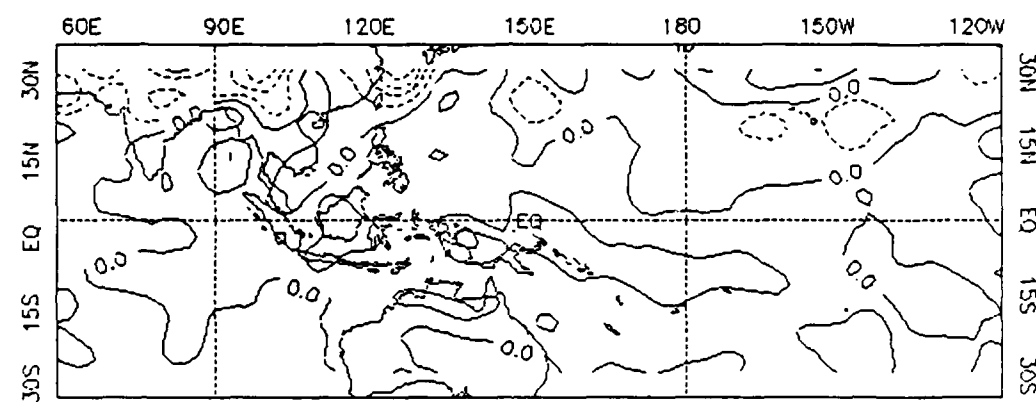


Figure 21. (a) Correlations, contour interval .2, (b) 200 mb divergence, contour interval of $2 \times 10^{-6} \text{ s}^{-1}$, (c) EBBI, contour interval 2 W m^{-2} .

(22a) Pattern Correlation for January



(22b) Mean January Divergence



(22c) Mean January EBBI

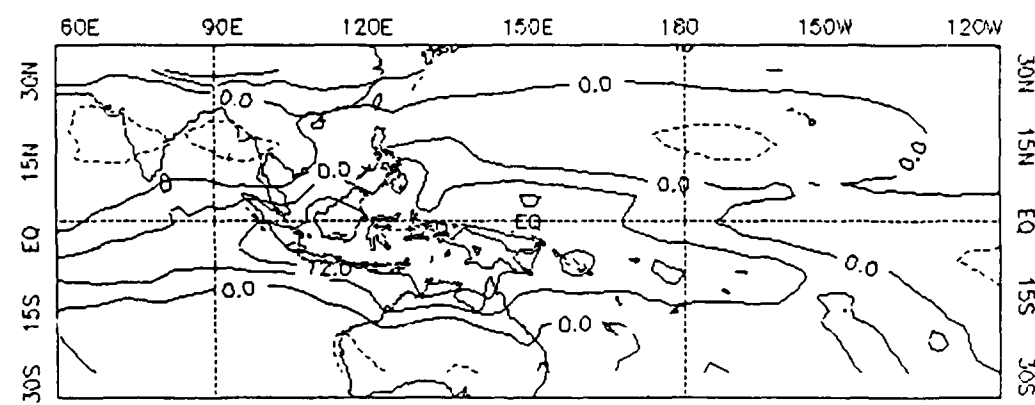
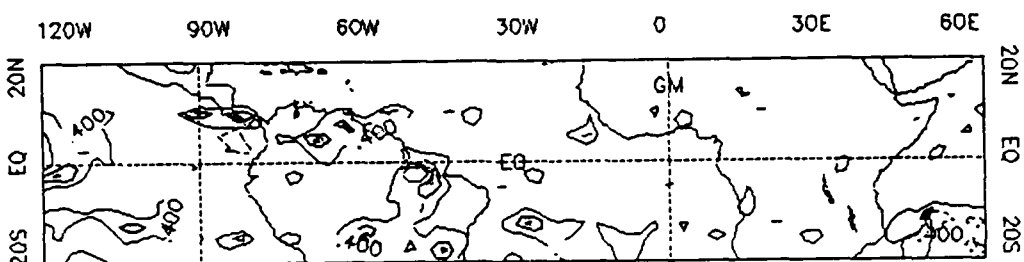
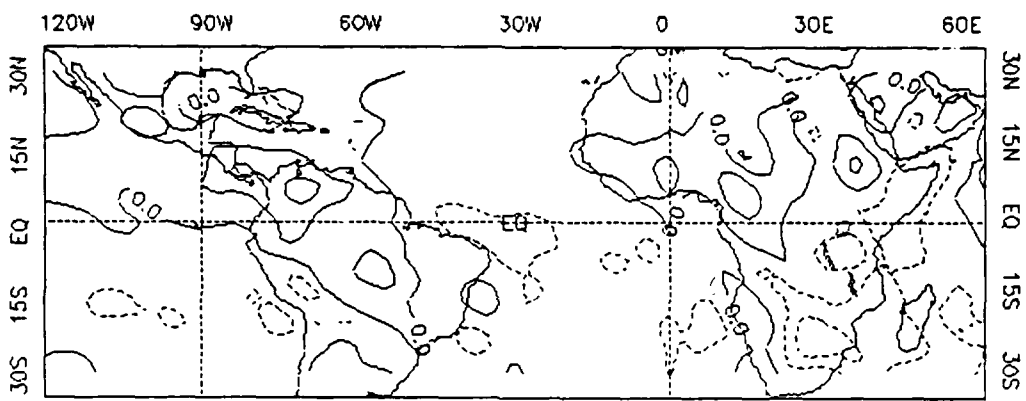


Figure 22. As in Figure 21.

(23a) Pattern Correlation for July



(23b) Mean July Divergence



(23c) Mean July EBBI

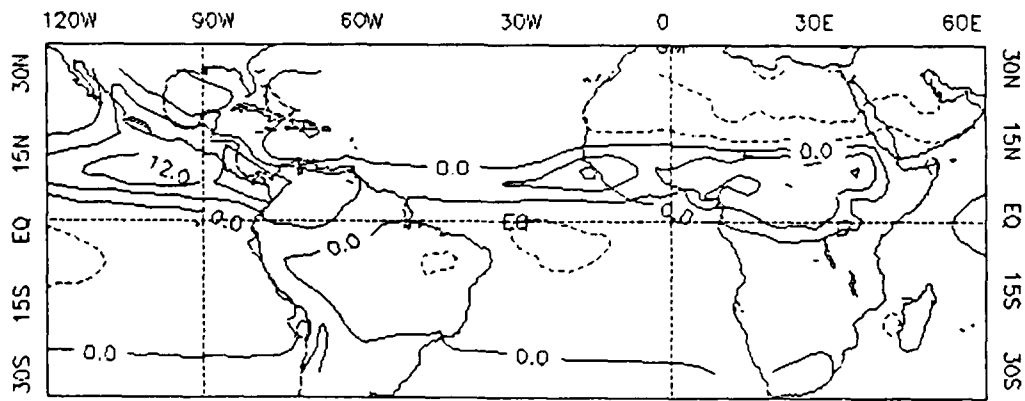
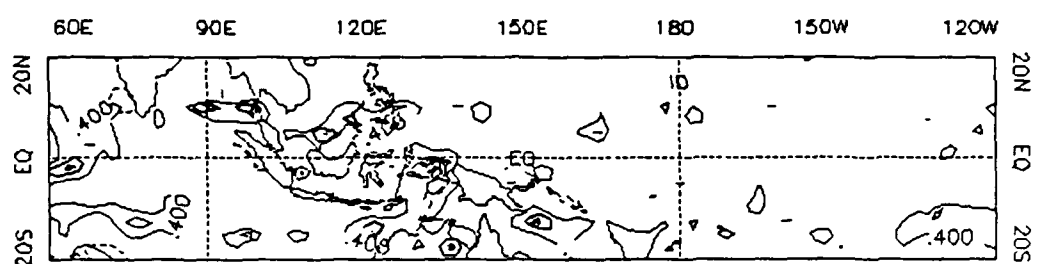
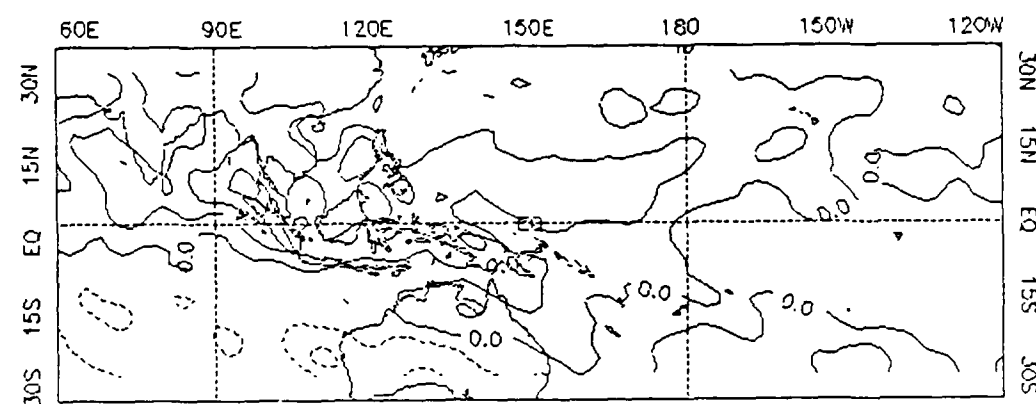


Figure 23. As in Figure 21 except for July.

(24a) Pattern Correlation for July



(24b) Mean July Divergence



(24c) Mean July EBBI

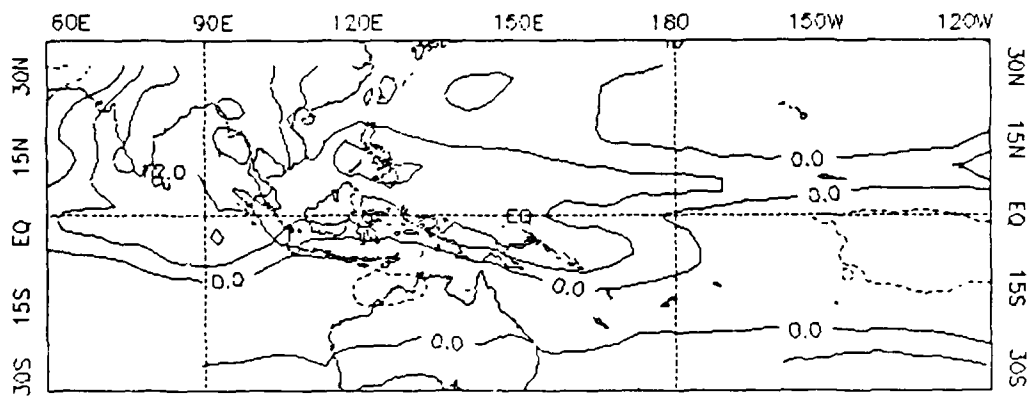


Figure 24. As in Figure 21 except for July.

7. Summary

We studied the variability of the 200 mb tropical irrotational wind field and its relationship to variabilities in OLR fluxes. Horizontal divergence is an important component of atmospheric circulations in the tropics. Until recent advancements in satellite derived data the measurement of divergent components was very limited. These improvements, along with timely studies of variations in tropical circulation by Bjerknes (1969) and Krishnamurti (1971a, 1971b, and 1973), were important to focusing research on this field.

Velocity potential and OLR flux data for the 8 years from January 1979 to December was provided by the NMC Climate Analysis Center. The extent of this data allowed us to examine intra- and inter-annual variabilities over an extended period. (Bjerkne's and Krishnamurti's work, cited above, were based on very limited data set) Other studies, such as Kasahara et. al. (1987a) and Julian (1984), studied the problem of quantifying the relationship between divergence and OLR flux fields. We also examined this problem.

Our first observation about the 200 mb tropical divergent velocity field is the dominance of the western Pacific source region associated with monsoon activity. This region drives both the meridional and zonal overturning motions. Smaller, but important source regions are found over South and Central America as well as Africa. The most important variation we observed concerning these source regions is their intra-seasonal transitions to the summer hemisphere. A second observation brought out by seasonally

averaged data was the variability in the NH flow while the SH had only slight variations. This hemispheric asymmetry is in response to differences in zonally asymmetric forcing features between the hemispheres. Our results, in general, compared favorably to those of Arkin et. al. (1986) and Lau and Boyle (1987) who studied similar variations in tropical circulations.

Intra- and inter-annual variations in the zonal mean meridional circulations indicated the same seasonal meridional transitions found in the seasonal means. In addition, the ascending and descending branches were clearly observed in the monthly mean data. Another feature was the strong annual cycle we found in the tropical belt from 30° N to 30° S and the seasonal fluctuations in the wind patterns driven by the ascending branch of the equatorial Hadley cell are quite clear. The winds shift from north to south in 6 month periods and this pattern remains spatially and temporally consistent over the entire 8 years with only magnitude variations associated with changes in the GDAS. These results were in general agreement with a study of zonal mean meridional tropical circulations by Oort and Rasmusson (1970).

The intra- and inter annual cycles of the mean zonal EBBI and divergence fields showed a strong relation between these independent data sets. Seasonal transitions and persistent annual cycles are reflected in both sets. The divergence field is noisier than the EBBI field. We expected this because the EBBI is very homogeneous in comparison to the divergence data.

Next we focused on the divergent motions on the zonal plane. We found strong evidence supporting the results of Krishnamurti (1973) that

the monsoon region is the source for east-west overturning motions in the tropics. In particular the Walker circulation in the equatorial Pacific was strongly supported by these fields. The east-west movements of the monsoon caused some variations in the spatial positioning of these motions. Again, on the inter-annual scale, the most striking feature was the persistence in annual cycles from year to year. This persistence held in the qualitative examination of the divergence and EBBI data.

One anomaly in the zonal mean flow which proved interesting was a noticeable anomaly in the inter-annual patterns of the zonal and EBBI fields. This happened during the El Nino period of late 1982 and 1983 in the central equatorial Pacific. Further investigation brought out clear variations between patterns prior to, and in the middle of, this event.

Finally we computed correlations between the divergence and EBBI data. Kasahara et. al. (1987) and Julian (1984) both have studied this relationship with only limited success. We were able to find a strong positive correlation in the latitudes close to the equator where convection is very strong. Conversely, we found very poor correlations as we moved further away from the equator. More specific correlations on a point-to-point basis for January and July data were less successful because only small areas of significant correlation were found.

This study, based on a relatively larger data set of tropical 200 mb divergent circulations than have been found elsewhere, confirmed the results of earlier works based on limited data. This study also contributed to understanding the intra- and inter-annual variations in these circulations.

The renewed interest in these circulations, and their importance to general circulation and numerical weather prediction, has occurred because of the wider availability of data. We feel continued research in this field is warranted because it is an important, yet unsolved, component of general circulation theory.

Appendix: Computational Techniques

1. Central Finite Differencing

The irrotational velocity vectors were calculated directly from the potential field using central finite differencing.

$$u_x = \frac{1}{a \cos \phi} \frac{\partial \chi}{\partial \lambda} = \frac{1}{a \cos \phi} \left(\frac{\chi_{i+1,j} - \chi_{i-1,j}}{2 \Delta \lambda} \right) \quad (13)$$

$$v_x = \frac{1}{a} \frac{\partial \chi}{\partial \phi} = \frac{1}{a} \left(\frac{\chi_{i,j+1} - \chi_{i,j-1}}{2 \Delta \phi} \right) \quad (14)$$

2. Zonal Averaging

Zonally averaged fields were computed as follows:

$$V_z(j) = \frac{1}{144} \sum_{i=1}^{144} v_{ij} \quad (j = 1 \dots 73) \quad (15)$$

where i represents the 144 longitudinal grid points from 0° to 360° , and j the latitudes from $90^\circ N$ to $90^\circ S$, each with 2.5° spacing interval. From this definition, the zonal average U_z equals zero:

$$U_z = \frac{1}{2\pi a \cos \phi} \int \frac{\partial \chi}{\partial \lambda} d\lambda = 0 \quad (16)$$

which shows no east-west momentum can accumulate around a latitude circle.

3. Divergence

The equations used to compute divergence $\nabla^2 \chi$ from the velocity

potential field follow:

$$\nabla^2 \chi = \frac{1}{a \cos \phi} \left(\frac{\partial u_\chi}{\partial \lambda} + \frac{\partial v_\chi \cos \phi}{\partial \phi} \right) \quad (17)$$

$$= \frac{1}{a \cos \phi} \left(\frac{\partial}{\partial \lambda} \left[\frac{1}{a \cos \phi} \frac{\partial \chi}{\partial \lambda} \right] + \frac{\partial}{\partial \phi} \left[\frac{1}{a} \frac{\partial \chi}{\partial \phi} \right] \cos \phi \right) \quad (18)$$

$$= \frac{1}{a^2 \cos^2 \phi} \left(\frac{\partial^2 \chi}{\partial \lambda^2} \right) + \frac{1}{a^2 \cos \phi} \left(\frac{\partial^2 \chi \cos \phi}{\partial \phi^2} \right) \quad (19)$$

We then used the following central differencing scheme:

$$\frac{\partial}{\partial \lambda} \left(\frac{\partial \chi}{\partial \lambda} \right) = \frac{\partial}{\partial \lambda} \frac{\chi_{i+\frac{1}{2},j} - \chi_{i-\frac{1}{2},j}}{\Delta \lambda} \quad (20)$$

$$= \frac{1}{\Delta \lambda} \left[\frac{\chi_{i+1,j} - \chi_{i,j}}{\Delta \lambda} - \frac{\chi_{i,j} - \chi_{i-1,j}}{\Delta \lambda} \right] \quad (21)$$

$$= \frac{1}{(\Delta \lambda)^2} \left[\chi_{i+1,j} + \chi_{i-1,j} - 2\chi_{i,j} \right] \quad (22)$$

Similar calculations can be made for $\frac{\partial}{\partial \phi} \frac{\partial \chi \cos \phi}{\partial \phi}$ to get:

$$\frac{\partial}{\partial \phi} \left[\frac{\partial \chi \cos \phi}{\partial \phi} \right] = \frac{1}{(\Delta \phi)^2} \left[(\chi \cos \phi)_{i,j+1} + (\chi \cos \phi)_{i,j-1} - 2(\chi \cos \phi)_{i,j} \right] \quad (23)$$

where on our 2.5° grid has: $\frac{1}{(\Delta \phi)^2} = \frac{1}{(\Delta \lambda)^2}$

4. Correlation

In section 6 we used several correlations which we will briefly describe here along with their significance test.

a. Type I used to compute Figures 17, 18, and 19.

1. In these figures we correlated the 8 year band-averaged mean grids for the divergence and EBBI fields.

Let \bar{x}_{ij} be the 8 year (96 month) mean over the entire domain. That is:

$$\bar{x}_{ij} = \frac{1}{96} \sum_{n=1}^{96} x_{ijn} \quad (24)$$

$$i = 1, \dots, 25 \text{ (Latitude)}, j = 1, \dots, 144 \text{ (longitude)}$$

The tropical grid goes from $30^\circ N$ to $30^\circ S$ (1,...,25 at 2.5° spacing interval) latitudes and from 0° to 357.5° (1,...,144 at 2.5° spacing interval) meridians. Next we computed the band average for the appropriate latitude belt:

$$A_j = \bar{x}'_j = \frac{1}{b-a} \sum_{i=a}^b (\bar{x}_{ij}) \quad (25)$$

$$j = 1 \dots 144$$

Finally, we compute the correlation between the Divergence and EBBI fields using the general correlation equation:

$$r = \frac{\sum_{j=1}^{144} (A_j - \bar{A})(B_j - \bar{B})}{\sqrt{\sum_{j=1}^{144} (A_j - \bar{A})^2 (B_j - \bar{B})^2}} \quad (26)$$

where A and B are mean fields computed as described above, and \bar{A} and \bar{B} are their means:

$$\bar{A} = \frac{1}{144} \sum_{j=1}^{144} A_j \quad (27)$$

2. t Test for significance:

$$t = \frac{r \sqrt{N-2}}{\sqrt{1-r^2}} \quad (28)$$

where $N=144$ and we get t at the 95% confidence level for $N-2$ degrees of freedom from tables. Here, $t_{95,142}$ equals 1.66. But all 144 values are not independent and hence it is not obvious what the degrees of freedom for

this case is and therefore no significance test was computed.

b. Type II, used to compute Figures 21 to 24.

1. In these figures we compute temporal correlations based on the 8 Januaries and the 8 Julies from 1979 to 1986. The tropical grid used in these figures was reduced to the latitudes from 20°N to 20°S which reduced the latitude index to i (1,...,17) First we computed the mean January and July fields then the 8 anomaly grids by subtracting the annual mean from the individual monthly grids and finally the correlations:

$$r_{ij} = \frac{\sum_{n=1}^8 [(X_{ijn} - \bar{X}_{ij}) (Y_{ijn} - \bar{y}_{ij})]}{\sqrt{(\sum (X_{ijn} - \bar{X}_{ij})^2) (\sum (Y_{ijn} - \bar{y}_{ij})^2)}} \quad (29)$$

2. The t test is used to check the significance at the 95% confidence level with $N = 8$, and $t_{95,6}$ equal to 2.447. This makes .70 the significant correlation level.

References

- Abel, P.G., and A. Gruber, 1979: An improved model for the calculation of longwave flux at 11 μm . NOAA Tech. Rep., NESS 106, 24 pp. [NTIS PB80-119431]
- Arkin, P.A., 1982: The relationship between interannual variability in the 200 mb tropical wind field and the Southern Oscillation. *Mon. Wea. Rev.*, 110, 1393-1404.
- Arkin, P.A., V.E. Konsky, J.E. Janowiak, and E.A. O'Lenic, 1986: Atlas of the tropical and subtropical circulation derived from National Meteorological Center operational analysis. U.S. Dept. of Commerce, NWS, Wash. D.C., NOAA Atlas No. 7, 28 pp.
- Bjerknes, J., 1969: Atmospheric teleconnections from the equatorial pacific. *Mon. Wea. Rev.*, 97, 163-172.
- Chang, C.P., and K.M. Lau., 1982: Short-term planetary interactions over the tropics and midlatitudes during northern DJF. Part I: Contrasts between active and inactive periods. *Mon. Wea. Rev.*, 110, 933-946.
- Cressman, G.P., 1981: Circulations of the west pacific jet stream. *Mon. Wea. Rev.*, 109, 2450-2463.
- Dey, C.H., and J.A. Brown Jr., 1976: Determination of a wind field on a sphere. U.S. Dept. of Commerce, NMC, Wash. D.C., NOAA Tech. Memorandum NMC-59, Apr., 14 pp.
- Dey, C.H., and L.L. Morone, 1985: Evolution of the national meteorological data assimilation system: January 1982-December 1983. *Mon. Wea. Rev.*, 113, 304-318.
- Dey, C.H., P.A. Phoebus, R.E. Kistler, A.J. Desmarais, J.J. Tuccilo, and B.A. Ballish, 1985: 1984 Summary of NMC operational global analysis. U.S. Dept. of Commerce, NMC, Wash. D.C., Office Note 309, Feb., 11 pp.
- Dey, C.H., B.A. Ballish, and P.A. Phoebus, 1987: 1985-1986 Summary of changes to NMC Operational Global Analysis. U.S. Dept. of Commerce.

NMC, Wash. D.C., Office Note 327, Mar., 25 pp.

Ellingson, R.A., and R.R. Ferraro, 1983: An examination of a technique for estimating the longwave radiation budget from satellite radiance observations. *J. Climate Appl. Meteor.*, 22, 1416-1423.

Gill, A.E., 1982: *Atmosphere - Ocean Dynamics*. New York: Academic Press, 662 pp.

Gruber, A., and A.E. Krueger, 1984: The status of the NOAA outgoing longwave radiation data set. *Bull. Amer. Meteor. Soc.*, 65 no. 9, 958-962.

Holton, J.R., 1979: *An introduction to dynamic meteorology*. New York: Academic Press, 2nd ed., 291 pp.

Hubert, L.F., and L.F. Whitney, Jr., 1971: Wind estimation from geostationary satellite pictures. *Mon. Wea. Rev.*, 99, 665-672.

Julian, P.R., 1984: Objective analysis in the tropics: A proposed scheme. *Mon. Wea. rev.*, 112, 1752-1767.

Kasahara, A., A.P. Mizzi, and U.C. Mohanty, 1987a: Comparison of global diabatic heating rates from FGGE Level IIIb analyses with satellite radiation imagery data. *Mon. Wea. Rev.*, 115, 2904-2935.

_____, R.C. Balgovind, and B.B. Katz, 1987b: Utilization of satellite radiometric imagery data for improvement in the analysis of divergent wind in the tropics. University Corporation for Atmos. Research, Boulder, Co., NCAR Report NCAR/0501/87-7, Jun., 38 pp.

Kistler, R.E., and D.F. Parish, 1982: Evolution of the NMC data assimilation system: September 1978 - January 1982. *Mon. Wea. Rev.*, 110, 1335-1346.

Krishnamurti, T.N., 1971a: Observational study of the tropical upper tropospheric motion field during northern hemisphere JJA. *J. Atmos. Sci.*, 10, 1066-1096.

-----, 1971b: Tropical east-west circulations during the northern JJA. *J. Atmos. Sci.*, 28, 1342-1347.

-----, 1973: Tropical east-west circulations during the northern DJF. *J. Atmos. Sci.*, 30, 780-787.

Lau, K.M., and J.S. Boyle, 1987: Tropical and extratropical forcing of the large-scale circulation: A diagnostic study. *Mon. Wea. Rev.*, 115, 400-427.

Lorenz, E.N., 1955: Available potential energy and the general circulation. *Tellus*, 7, 157-167.

Mohanty, U.C., A. Kasahara, and R. Errico, 1986: The impact of diabatic heating on the initialization of divergent circulations in a global forecast model. *J. Atmos. Soc. Japan*, 64, 805-817.

Ohring, G. and A. Gruber, 1984: Satellite determination of the relationship between total longwave flux and infrared window radiance. *J. Climate Appl. Meteor.*, 23, 416-425.

Oort, A.H., 1964: On estimates of the atmospheric energy cycle. *Mon. Wea. Rev.*, 92, 483-493.

Oort, A.H., and E.M. Rasmusson, 1970: On the annual variation of the monthly mean meridional circulation. *Mon. Wea. Rev.*, 98, 423-441.

Paegle, J.J., and J. N. Paegle, 1978: On the generation of large scale divergent winds and related energetics. *The General Circulation: Theory, Modeling, and Observations*, Notes from a Colloquium: JJA 1978, National Center for Atmos. Research, Boulder, Co., NCAR/CQ-6+1978-ASP, 236-248.

Ramanathan, V., and B.P. Briegleb, 1980: Special nature of cloud radiative feedback effects: Implications for interpretations of cloud effects from satellite measurements. *Proc. 1980 Int. radiation Symposium*, Fort Collins, LAMAP/IUGG, 355-357.

Richards, F., and P.A. Arkin, 1981: On the relationship between satellite-observed cloud cover and precipitation. *Mon. Wea. Rev.*, 109, 1081-1093.